INL/RPT-22-68581
Rev. 1

Light Water Reactor Sustainability Program

Safety Analysis for Accident-Tolerant Fuels with Increased Enrichment and Extended Burnup

August 2022

U.S. Department of Energy

Office of Nuclear Energy

INL/RPT-22--68581
Rev. 1

Safety Analysis for Accident-Tolerant Fuels with Increased Enrichment and Extended Burnup

Yong-Joon Choi[1]
Kingsley Ogujiuba[2]
Nicholas Rollins[2]
Khang Nguyen[2]
Jason Hou[2]
Una Baker[3]
Ben Lindley[3]

[1]Idaho National Laboratory, [2]North Carolina State University,
[3]University of Wisconsin-Madison

August 2022

Prepared for the
U.S. Department of Energy
Office of Nuclear Energy

Page intentionally left blank

EXECUTIVE SUMMARY

The United States (U.S.) nuclear industry is facing a strong challenge to maintain regulatory-required levels of safety while ensuring economic competitiveness to stay in business. Safety remains a key parameter for all aspects related to the operation of light water reactor (LWR) nuclear power plants (NPPs), and it can be achieved more economically by using a risk-informed ecosystem, such as that being developed by the Risk-Informed Systems Analysis (RISA) Pathway under the U.S. Department of Energy (DOE) Light Water Reactor Sustainability (LWRS) Program. The LWRS Program is promoting a wide range of research and development (R&D) activities with the goal to maximize both the safety and economically efficient performance of NPPs through improved scientific understanding, especially given that many plants are considering second license renewal.

The RISA Pathway has two main goals: (1) the deployment of methodologies and technologies that enable better representation of safety margins and the factors that contribute to cost and safety; and (2) the development of advanced applications that enable cost-effective plant operation.

As part of RISA Pathway, Enhanced Resilient Plan (ERP) project refers to an NPP where safety is improved by implementation of various measures, such as accident-tolerant fuels (ATF), diverse and flexible coping strategy (FLEX), enhancements to plant components and systems, incorporation of augmented or new passive cooling systems, and utilization of advanced battery technologies. The objective of the ERP research is to use novel methods and computational tools to enhance existing reactors' safety while reducing operational costs.

The ERP R&D efforts in fiscal year (FY) 2022 focused on safety analyses of ATFs with increased enrichment and extended burnup to provide scientific knowledge of the ATF fuel performance, failure mechanisms, and resulting from fuel failure source terms during a severe accident. FeCrAl clad ATF was the focus of this research. An optimized equilibrium cycle was developed for a 24-month extended burnup operation for a generic 4-loop pressurized water reactors (PWR) model. The consequences of a loss-of-coolant accident (LOCA) was assessed and the major source term from the failed ATF was analyzed. ATF loaded core shown less failure rate and smaller amount of major radioactive material released compared to Zr-clad fuel core.

Page intentionally left blank

CONTENTS

FIGURES

TABLES

ACRONYMS

ANS	American Nuclear Society
AOO	Anticipated Operational Occurrences
ATF	Accident-Tolerant Fuel
BDBA	Beyond-Design Basis Accident
BOC	Beginning of Cycle
BWR	Boiling Water Reactor
DBA	Design Basis Accident
DOE	Department of Energy
ECCS	Emergency core cooling system
EFPD	Effective Full Power Day
EOC	End-of-Cycle
EOEC	End-of-Equilibrium-Cycle
ERP	Enhanced Resilient Power plant
FCA	FeCrAl (iron-chromium-aluminum)
FFRD	Fuel Fragmentation, Relocation and Dispersal
FLEX	Diverse and Flexible Coping Strategy
FY	Fiscal Year
HBU	High Burnup
IFBA	Integrated Fuel Burnable Poison
INL	Idaho National Laboratory
LBLOCA	Large Break Loss-Of-Coolant Accident
LOCA	Loss-Of-Coolant Accident
LPSI	Low-pressure safety injection
LWR	Light Water Reactor
LWRS	Light Water Reactor Sustainability
M&S	Modeling and Simulation
NPP	Nuclear Power Plant
NRC	U.S. Nuclear Regulatory Commission
NUREG	Nuclear Regulatory Report
OECD	Organization for Economic Cooperation and Development
ORNL	Oak Ridge National Laboratory
PWR	Pressurized Water Reactor
R&D	Research and Development

RISA	Risk-Informed System Analysis
SNL	Sandia National Laboratory
SOARCA	State-of-the-Art Reactor Consequence Analyses
TH	Thermal-hydraulics
TRISO	Tristructural isotropic
U.S.	United States
UDM	User-Defined Material
WABA	Wet Annular Burnable Absorber
WBN	Watts Bar Nuclear power plant

1. INTRODUCTION

The United States (U.S.) Department of Energy (DOE) Light Water Reactor Sustainability (LWRS) Program Risk-Informed Systems Analysis (RISA) Pathway Enhanced Resilient Plant (ERP) aims to enhance both the safety and economics of existing nuclear power plants (NPPs) using advanced, near-term technologies that provide substantial improvements to plant safety margins. The project supports the DOE and industry initiatives targeting improvements of the safety and economic performance of the current fleet of NPPs such as accident-tolerant fuel (ATF), diverse and flexible coping strategy (FLEX), passive cooling system designs, and advanced battery technologies. The concept of ERP refers to a NPP where safety is improved by implementation of various measures such as those described above. The objective of the ERP research is to use novel methods and computational tools to enhance existing reactors' safety while reducing operational costs. Until fiscal year (FY) 2021, the project focused on assessments of safety benefits from the combination of ATF, FLEX, passive cooling, and new battery technologies. The research provided important information to the NPP owners and operators as to what plant enhancements are most beneficial in terms of increased safety margins. The work also identified additional opportunities to further increase safety margins, which is the focus of the future research. From FY 2022, the project advanced to focus on safety assessments of ATFs with increased enrichment and extended burnup, which is an urgent near-term industry initiative that offers enhancements of safety as well as economic gains. This work could serve as a roadmap for safety analyses that NPPs must include in their license amendment requests supporting the use of new fuels.

As of 2022, most of U.S. pressurized water reactors (PWR)[1] operate on an 18-month cycle but many NPPs are interested in a longer refueling cycle (e.g., 24-month) which can be accomplished by increased uranium enrichment and higher burnup (HBU) resulting from fuel remaining in the reactor core longer. The longer refueling cycle offers substantial economic gains which help to offset higher ATF costs. However, increasing the cycle length from 18 to 24 months requires an increase of the regulatory limits on fuel enrichment and discharge burnup [1]. The increase of the cycle length and burnup limit also increases risk of fuel failure due to a design basis accident (DBA). With the prolonged residence of the fuel in the core, the integrity of the fuel diminishes which results in pellet cracking and subsequent release of fission product gases. This also corresponds to an increase in the plenum pressure and in turn additional stresses on the cladding including increased corrosion and hydrogen uptake. The major fuel degradation phenomenon is called fuel fragmentation, relocation, and dispersal (FFRD). This failure mechanism can be observed during postulated accident events and may cause fuel damage exceeding the postulated safety limits. Multiple research efforts have been dedicated to investigation of the FFRD phenomenon and its consequences. However, most of them were focused on conventional fuel (e.g., non-ATF). The recent study by the U.S. Nuclear Regulatory Commission [2] addressed that fuel fragmentation can be observed starting from 55 GWD/MTU burnup (average burnup of U.S. NPP is 45 GWD/MTU) for standard UO_2 fuel during a design basis loss-of-coolant accident (LOCA). NRC also noted that existing FFRD regulation is not applicable for burnup higher than 68 GWD/MTU since HBU rod internal pressure may exceed initial rod internal pressure. Existing fuel-cladding interaction model will not be applicable for FFRD in HBU fuels [3]. Safety analyses of higher enriched ATFs with extended burnup operations are still incomplete especially in terms of FFRD. New experiment is planned to understand FFRD behavior at HBU fuels [4].

Generally, ATFs have advantage of better mechanical strength under high-temperature accident conditions over the traditional fuel (i.e., zircalloy cladding). It has been established that relatively modest improvements in severe accident performance can be achieved through ATF [5]; however, ATFs have the potential to recover margin with respect to conventional fuel and therefore enhance plant economics. In

[1] Most of existing boiling water reactors (BWR) are currently operate on a 24-month cycle.

this context, extended burnup operation up to 24-month cycle can provide a significant economic benefit for operating nuclear reactors.

The ATF chosen for this project was iron-chromium-aluminum (FeCrAl or FCA) clad combined with conventional uranium dioxide fuel. FeCrAl is a promising ATF concept due to improved oxidation resistance, lower hydrogen generation rate, and the potential for improved coping time available for quenching compared to Zircaloy [6]. There is significant previous and ongoing work on the analysis of design basis accidents in codes (for example [7] and [8]). Recent work has also considered the impact of FeCrAl cladding and Cr_2O_3-coated Zircaloy cladding on severe accidents in LWRs, showing the potential for modest additional coping time [9] and [10] although otherwise similar consequences. This motivates the investigation of beyond-design basis accidents of recovered LOCAs, where additional coping time may prove beneficial. However, the increase in coping time is limited to the order of minutes to hours depending on the transient under consideration [10]. A sensitivity analysis was performed on the response to various beyond-design basis accidents using the TRACE code with FeCrAl-clad compared to Zircaloy clad, varying the time at which the safety injection systems were recovered and quantifying coping time [11].

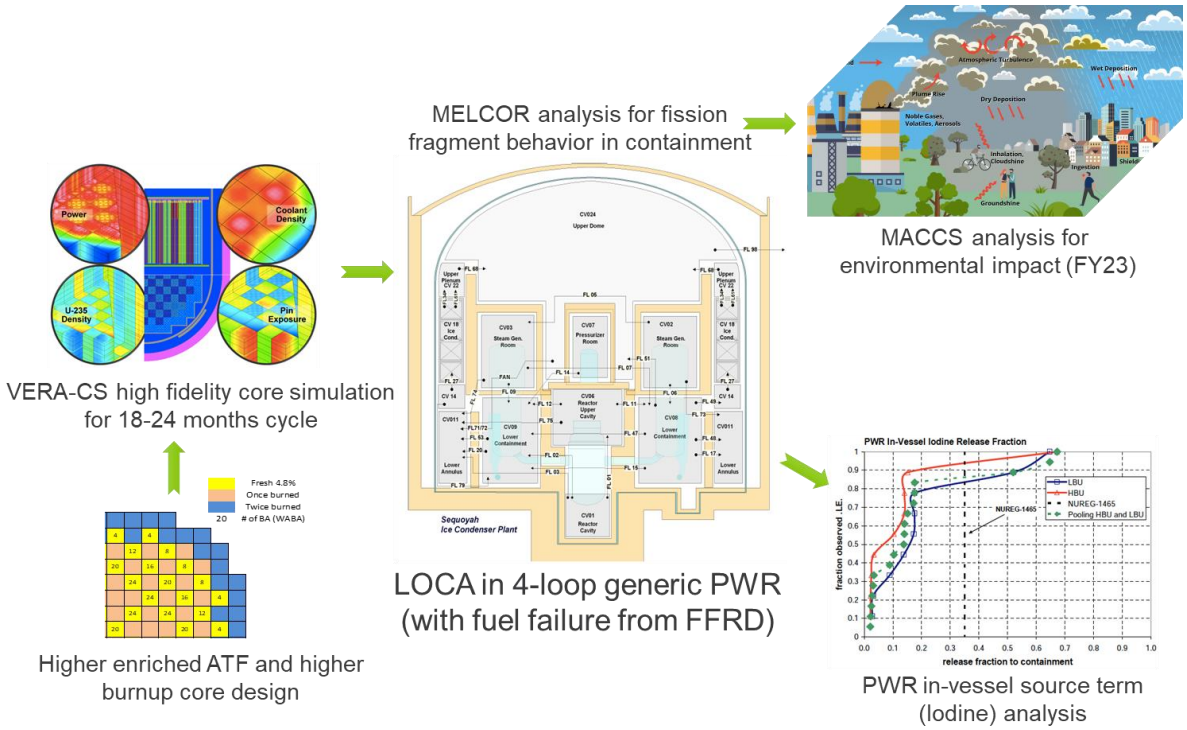

Figure 1-1. Schematic diagram of ATF loaded PWR with extended burnup safety analysis.

The research scope includes the development of optimized reactor core configuration with ATF specific to a 24-month cycle, fuel behavior analysis with respect to the FFRD phenomenon, source term evaluation, and consequence analysis. Neutronics analyses were carried out to evaluate the reactivity penalties introduced by the FeCrAl cladding in various fuel pin configurations during the lifetime of the fuel. Optimal reactor core designs filled with both zirconium (Zr) alloy and FeCrAl-clad fuel rods were obtained using the multi-objective optimization method coupled with modeling and simulation (M&S) capabilities to maximize the equilibrium cycle performance. Figure 1-1 shows schematic diagram of the analysis framework. The FeCrAl loaded PWR reactor core was designed based on the Watts Bar Nuclear (WBN) power plant Unit 1. The reactor core was design by using POLARIS/PARCS suite [12] then the equilibrium cycle depletion calculation was performed by VERA-CS high-fidelity reactor simulation environment [13]. VERA-CS uses a one-step method with its use of multigroup cross sections and multi-

physics coupling algorithms for explicit pin-by-pin transport solutions. The one-step method is characterized by explicit pin-by-pin powers and burnup, pin local thermal-hydraulic distributions and significant runtime while the two-step method has pin power reconstruction for power and burnup distribution, node-averaged quantities, and a much faster runtime than its one-step counterpart.

The result of reactor simulation from VERA-CS is then sent to MELCOR [14] the severe accident analysis tool for the source term analysis. MELCOR is a fully integrated, engineering-level computer code developed for the Nuclear Regulatory Commission (NRC) whose primary purpose is to model the progression of accidents in LWR NPPs. A LOCA of the typical Westinghouse 4-loop PWR was simulated under the assumption of a failure of the automatic actuation of the emergency core cooling system (ECCS) with operator manually starting the low-pressure safety injection (LPSI) system at 27 minutes from the reactor trip. The analysis focused on the fission fragment, the source term, and behavior of the released radiological material in the reactor containment. The environmental impacts will be analyzed in FY 2023 by using MACCS [15], the accident consequence evaluation code.

1.1 Source Term Evaluation during Severe Accident

The source term refers to the released radioactive materials in postulated accident as defined in 10CFR Part 100: Reactor Site Criteria [16]. The existing regulatory guidance is NUREG-1465 which is often called "NUREG-1465 Source Term" [17]. Five severe accident source term release phases were defined as follows:

- Coolant radioactivity[2] release
- Gap radioactivity release
- Early in-vessel release
- Ex-vessel release
- Late in-vessel release

In case of postulated accident, the radioactive reactor coolant will be released to the containment through the break or leak in the reactor coolant system. As accident progresses, radioactivity in the fuel gap will be released to the coolant through failed cladding and followed by melting of the fuel and core materials. In this early in-vessel release phase, significant amount of the noble gases and fission products will be released into the reactor containment. The molten core (i.e., corium) will penetrate the reactor vessel bottom head during the ex-vessel release phase which generates large quantities of non-radioactive aerosols from molten core-concrete interactions. On a longer timeframe, there will be late in-vessel release of volatile nuclides which were deposited in the reactor coolant system.

Table 1-1 and Table 1-2 show list of the source term radionuclide groups to be considered during DBA analyses and release limits to the containment during the PWR postulated accidents, respectively [17]. The values of source term in Table 1-2 show fractions of initial core fission product inventory. In case of long-term cooling the gap release fraction will be up to 3%.

For the fission product release, which is major part of the source term, two different phenomena are important [18]. The first called "high pressure melt ejection". If the reactor coolant system was at high pressure when vessel bottom head failed, the molten core will be ejected to the containment with high velocity. This will lead rapid increase of in-containment temperature as well as aerosol type source terms. Another phenomenon is molten core debris release as airborne fission product from the large-scale steam explosion as a result of interaction between molten core and water. Small size steam explosion will likely

[2] NUREG-1465 used the term "activity".

occur but negligible in increasing source term, but large-scale explosion will ease release of molten core debris within the vapor and water droplets.

Table 1-1. Radionuclide groups in source term [17].

Group	Element
Noble gases	Xe, Kr
Halogens	I, Br
Alkali metals	Cs, Rb
Tellurium group	Te, Sb, Es
Barium, Strontium	Ba, Sr
Noble metals	Ru, Rh, Pd, Mo, Tc, Co
Lanthanides	La, Zr, Nd, Eu, Nb, Pm, Pr, Sm, Y, Cm, Am
Cerium group	Ce, Pu, Np

Table 1-2. Source term release limitation to the containment in PWR DBAs [17].

	Gap release	In-vessel	Ex-vessel	Late in-vessel
Duration (hours)	0.5	1.3	2.0	10.0
Noble gases	0.05	0.95	0	0
Halogens	0.05	0.35	0.25	0.1
Alkali metals	0.05	0.25	0.35	0.1
Tellurium group	0	0.05	0.25	0.005
Barium, Strontium	0	0.02	0.1	0
Noble metals	0	0.0025	0.0025	0
Lanthanides	0	0.0002	0.005	0
Cerium group	0	0.0005	0.005	0

The amount of source term during the severe accident in each phase was first calculated by MELCOR code for 40 to 62 GWD/MTU burnup PWR [19] and BWR [20]. In these studies, various of postulated accidents were considered to evaluate source term release time and amounts. The result of these study became reference data to set NRC guide and DG-1389 (1.183 rev 1) [21].

The source term from the Fukushima type BWR with FeCrAl cladding fuel was evaluated under DBA and beyond-design basis accident (BDBA) [22]. In DBAs, less oxidation and higher heat capacity of ATF benefits of reducing peak cladding temperatures (PCT) significantly, either ECCS injection is delayed or even not activated. However, in case of BDBA, higher melting point and less oxidation will not preclude a severe accident if core cooling cannot be restored.

1.2 Overview of Accident-Tolerant Fuel

1.2.1 Background

In the current nuclear fleet, the commercial nuclear fuels available are majorly made up of enriched fuels packed into UO_2 pellets with a zirconium based cladding design. While the use of this fuel type has its advantages, such as low-thermal absorption cross section, reasonable corrosion resistance, and good mechanical properties under normal operation and neutron irradiation, key factors that affect the degradation of the zirconium claddings are radiation swelling and embrittlement caused by oxidation and hydrogenation [23] and [24]. The satisfactory performance of this fuel type was challenged during the Fukushima Daiichi accident in 2011. In this accident, the loss of active core cooling system led rapid temperature increase and converted the coolant water to steam. This resulted in a severe degradation of the cladding due to rapid oxidation with high-temperature steam accompanied by the generation of high amounts of heat and hydrogen. As a result, this accident highlighted the inherent weakness of the Zr-based alloy claddings [25]. Following this disaster, the nuclear community has made efforts to ensure safe operation and accident management of nuclear plants and to engineer a successor to the current UO_2-Zr fuel-cladding system, which can minimize hydrogen risk during a severe accident [26]. While significant progress has been made, there is still a need for new fuel concepts that enhance or maintain fuel performance under normal and transient operating conditions, as well as during a potential DBA BDBA [27].

The new fuel concepts, or ATFs, are designed to combat some of the perceived disadvantages of the UO_2-Zr-based fuel. Some of these concepts include specially designed additives to standard fuel pellets and robust coatings applied to the outside of standard Zr claddings. They are intended to reduce corrosion, increase wear resistance, and reduce the production of hydrogen under severe accident scenarios. Consequently, ATF have shown better endurance in the case of a loss of active reactor core cooling for a longer time than the current zirconium fuel. To varying degrees, the ATF designs offer more flexibility in the operation of NPPs and provide more robust performance during normal operations and potential accident scenarios. Most notably, ATF designs mitigate accidents by offering plant operators additional time prior to the onset of potential fuel damaging conditions. The ATF designs also can reduce the production of high-level waste in the reactor by offering extended operation of fuel assemblies in the reactor core.

1.2.2 Categories of Accident-Tolerant Fuels

Over the years, materials research has been performed towards the development of several high-performance systems with improved fuel performance characteristics. In these cases, fuel thermal conductivity, as one of the key factors of the reactor design and safety, governs the conversion of heat produced from fission reaction into electricity. Most important parameters are fuel performance and behavior, such as grain growth, fission gas release, fission products migration, and swelling under normal and transient conditions. A variety of approaches have been considered as potential accident-tolerant alternatives to Zr alloy cladding and in all cases, the desired accident-tolerant attributes are improved high-temperature oxidation resistance and comparable or superior high-temperature strength [24]. These approaches can be either classified as advanced fuel claddings or advanced fuel pellets.

1.2.2.1 Advanced Fuel Cladding

In 2018, OECD Nuclear Energy Agency reviewed five different types of cladding designs: coated and improved Zr alloys, advanced steels, refractory metals, SiC and SiC/SiC-composite claddings, and non-fuel components such as channel boxes and accident-tolerant control rods [28]. However, this study focuses only on the cladding designs developed for fuel components.

One type of advanced fuel cladding is coated Zr alloys. These include robust coatings to the outer layer of the current zirconium claddings with the intention of reducing corrosion or increasing wear

resistance. Several coating materials such as chromium have been investigated and with sufficient thickness, the mechanical properties are modified with enhanced strength and reduced ductility [29], [30]. The main advantage of the coated cladding is that while it preserves the benefits of the base zirconium such as the low-thermal absorption cross section and mechanical properties, it also improves its oxidation and corrosion resistance in accident conditions.

Another option for the advanced fuel cladding is the oxidation-resistant structural alloys, such as advanced steels, which offer the potential for improved strength and oxidation resistance compared to Zr alloys over a broad temperature range [24]. These advanced steels include ferritic and martensitic steel alloys with the most noticeable example being the FeCrAl alloy cladding [31]. These developed alloys are highly corrosion resistant due to the formation of a thin aluminum oxide layer. While the FeCrAl alloy has superior mechanical strength in comparison to Zr alloy cladding, two main disadvantages of this alloy are its increased parasitic neutron absorption due to the presence of iron in the alloy and increased tritium release into the reactor coolant.

Refractory steels offer the potential for significant improvements in high-temperature strength to Zr alloys. Although these alloys generally exhibit poor behavior in high-temperature oxidizing environments, research has identified some alloys such as molybdenum alloy with adequate short-term oxidation resistance.

SiC matrix ceramic composites (SiC/SiC) are another option for advanced fuel cladding because of their low-thermal neutron absorption cross section, retention of strength up to elevated temperatures, good radiation and oxidation resistance in the air and steam up to temperatures of 1600°C [28]. While these advantages make it a suitable option, it also has its disadvantages, such as fabrication, tritium releases, and lower thermal conductivity than zirconium alloys, which negatively affect the fuel centerline temperature.

1.2.2.2 Advanced Fuel Pellets

Advanced fuel designs mainly consist of three concepts: the improved UO_2 fuel, high-density fuel, and tristructural isotropic (TRISO)-SiC-composite pellets [28]. The first design is related to the addition of a ceramic or metallic dopant to the fuel. This concept, referred to as the improved UO_2 fuel, consists of both oxide-doped UO_2 and high-thermal conductivity UO_2. The dopants added to the pellet improve the fuel performance by enhancing the retention of the fission products and minimizing pellet-cladding interaction. In addition, the inclusion of these dopants can increase the thermal conductivity of the fuel pellet, as low-thermal conductivity can result in localized overheating in the fuel centerline.

A second design option for ATFs includes high-density materials, such as nitride fuels, silicide fuels, carbide fuels, and metallic fuels [28]. The fuel density is increased to compensate for the reactivity penalties introduced by the alternative metallic materials without conceding either the ^{235}U enrichment or cycle length. The fuel density can be increased by increasing the material density or by increasing the metal-to-non-metal ratio in the metal compound fuels. The benefits of such fuels are the improved retention of fission products via introduction of one or more additional safety barriers for fission product release.

The third fuel concept is an encapsulated fuel design. This design moves away from the traditional pellets to micro-fuel particles consisting of fissile material bearing kernels with multiple coatings of dense or porous silicon carbide. Also known as TRISO-SiC-composite pellets, they are made of TRISO particles embedded in a SiC matrix, which improves the fission product retention and radiation tolerance of the fuel under most conditions [28].

1.2.3 FeCrAl Cladding

The iron-based cladding (i.e., FeCrAl alloy) shows good corrosion, oxidation resistance, and high-mechanical strength when compared to the zirconium alloy [31][34]. Generally developed for

industrial applications where high-temperature oxidation is common, the oxidation resistance increases with increasing amounts of chromium and aluminum additions in the alloy. Compared with the Zr alloy-based cladding, some prominent characteristics of the FeCrAl cladding include reduced fuel-cladding thickness to provide more fuel volume, greater corrosion resistance even at high temperatures, improved high-temperature steam oxidation resistance, as well as improved strength at normal operations and accident conditions. Other advantages of this cladding material are its improved normal operation corrosion performance and lack of reaction with hydrogen to form stable hydrides, which improves cladding ductility. However, the lack of stable hydrides results in higher permeability of the fission product tritium through the cladding to the reactor coolant and steps must be taken to mitigate this issue [28].

Table 1-3. FeCrAl alloy iterations for nuclear applications.

Alloy Designation	Vendor	Nominal Composition (wt.%)
C26M	ORNL	Fe-12Cr-6Al-2Mo-0.2Si-0.05Y
Kanthal APMT	Kanthal	Fe-21Cr-5Al-3Mo
C35M	ORNL	Fe-13Cr-5Al-2Mo-0.2Si-0.05Y
Kanthal A-1	Kanthal	Fe-21Cr-5.8Al
561	GE	Fe-5Cr-6Al-1Y
1041	GE	Fe-10Cr-4Al-1Y
C35M01TC	ORNL	Fe-10Cr-5Al-2Mo-0.2Si-0.05Y+0.1TiC*

*TiC was added to the base C35M case as a hydrogen getter to improve fuel performance

Variations of the FeCrAl alloys have been developed by commercial entities, universities, and national laboratories over the years with varying Cr (typically 5–15 wt.%) and Al (3–6 wt.%) content. Table 1-3 gives a list of the FeCrAl alloys developed by different vendors and their compositions. This table lists not just the base cases of the alloy configuration but also some of the variations of this base case, developed by the addition of a different substance to the base alloy configuration.

The alloy composition, classified as “nuclear grade,” is an optimized composition developed to perform in both normal and off-normal conditions of a nuclear power plant [31]. Small quantities of select atoms or molecules are added to the base configuration of these alloys, which try to improve fuel performance by improving specific characteristics of the alloy.

For this study, the Kanthal APMT alloy composition was selected based on the availability of its properties in literature and for consistency with other M&S tools. The nominal chemical composition of the Kanthal APMT alloy is 3wt.% Mo, 21wt.% Cr, 5wt.% Al, and 71wt.% Fe. In addition to the nominal configuration of the alloy, certain elements are added to this base alloy to further improve specific fuel performance aspects. Table 1-4 shows nominal composition of element and their minimum and maximum atomic weight percentages of Kanthal APMT.

Under normal operating conditions, a thin layer of Cr_2O_3 forms on the surface of the FeCrAl cladding. At higher temperatures, this chromium oxide layer evaporates and forms a protective Al_2O_3 layer. If the temperature continues to rise past 1773K, this aluminum oxide layer also fails, and oxidation begins. It is noted that the thickness of the FeCrAl cladding is assumed to be equal to that of the Zircaloy clad, for consistency with the complementary reactor physics analysis being performed elsewhere in the project.

Table 1-4. The chemical composition (wt.%) of the Kanthal APMT FeCrAl material.

Element	C	Si	Mn	Mo	Cr	Al	Fe
Nominal				3.0	21.0	5.0	Balance
Min	–	–	–		20.5	–	
Max	0.08	0.7	0.4		23.5	–	

2. REACTOR CORE AND EQUILIBRIUM CYCLE DESIGN

2.1 Reactor Core Specification

The generic reactor used in this research for core and cycle design is a four-loop PWR based on the WBN-1 reactor core [34]. This core is filled with 193 fuel assemblies and has a rated thermal power of 3,411 MW. Main operating parameters of this core are shown in Table 2-1. Figure 2-1 shows the diagram of the WBN-1 Cycle 1 full-core layout on the left with an axial layout of the fuel assembly on the right.

Table 2-1. Core characteristics for the generic PWR.

Parameter	Value
Rather thermal power (MWth)	3,411
Rated Flow (kg/s)	18,231
Inlet Temperature (K)	565
Coolant Average Temperature (K)	585
System Pressure (MPa)	15.51
Coolant Core Bypass Flow rate (%)	9.0

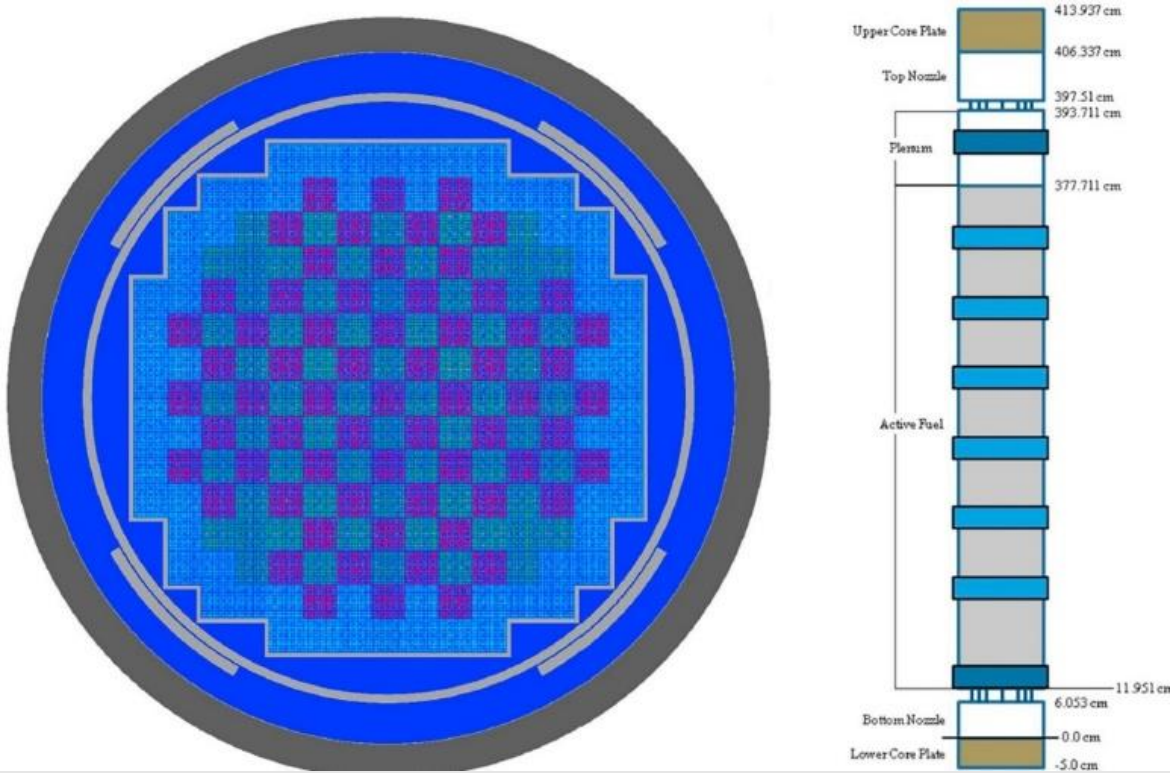

Figure 2-1. Watts Bar Nuclear Unit 1 core diagram [34].

2.1.1 Fuel Assembly Specifications

The fuel assembly used in this analysis consists of a 17×17 lattice of fuel rods. It is 21.50 cm wide and 406.337 cm tall, containing 264 fuel rods arranged in an orthogonal array with six intermediate spacer grids and two end grids. The assembly also contains 24 guide tubes. Table 2-2 lists the fuel assembly geometry specifications with the nominal cladding thickness calculated to be 0.0572 cm.

Table 2-2. Fuel assembly geometry specifications.

Specification	Value
Fuel density (g/cc)	10.257
Assembly pitch (cm)	21.50
Rod pitch (cm)	1.26
Fuel pin radius (cm)	0.4096
Inner clad radius (cm)	0.4178
Outer clad radius (cm)	0.4750
Inner guide tube radius (cm)	0.5610
Outer guide tube radius (cm)	0.6020

2.1.2 Core Design Specifications

The 17×17 assembly design is fueled with UO_2 fuel, clad in either Zr alloy or Kanthal APMT FeCrAl alloy. The fuel pins have an active stack height of 356.76 cm with 152.4 cm solid axial blankets of 2.61 wt.% enrichment at the top and bottom of the active fuel length. The reactor core is loaded with 84 fresh assemblies in a 3-region, 2-batch cycling scheme. These batches contain different numbers of Integrated Fuel Burnable Poison (IFBA) and Wet Annular Burnable Absorber (WABA) coated fuel rods, which is consistent with WBN-1 reactor. It is noted that the position of the WABA is not constrained, and future effort is needed to set correct position of WABA rods for the FeCrAl-clad fuel assemblies.

Optimal core designs are generated with a select assembly design options, which reduces the scope of the optimization. In addition, mirror one-eighth symmetry boundary conditions are applied to further limit the search space. The base core loading pattern is shown in Figure 2-2.

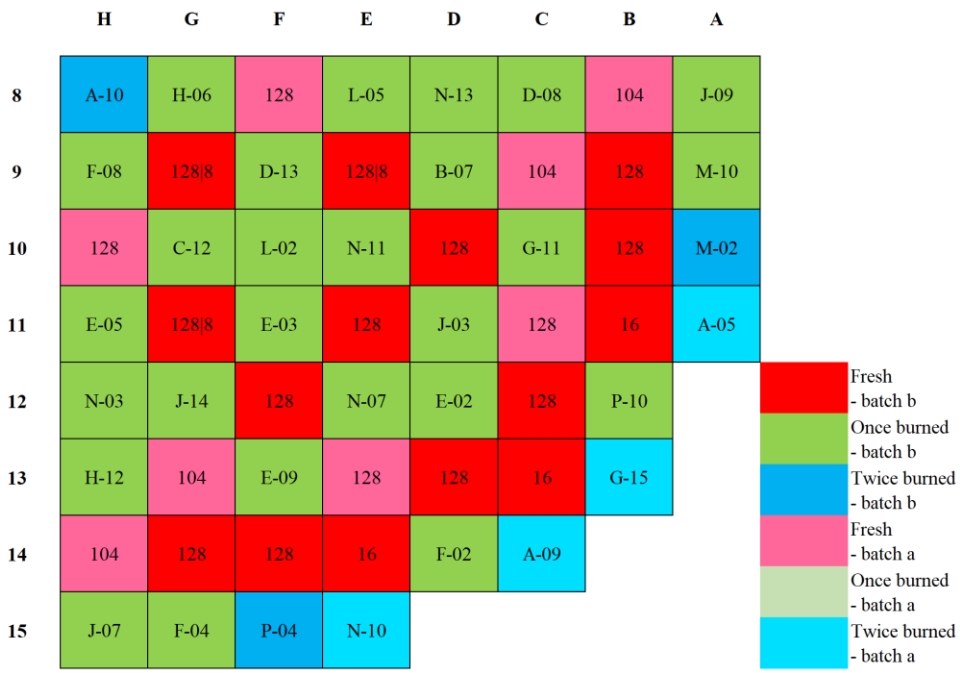

Figure 2-2. Core configuration and loading pattern for reference core design.

2.1.3 Designing Optimized FeCrAl PWR Core

A FeCrAl loaded optimized PWR reactor core was designed to be used for the equilibrium cycle. The core is filled with either Zr alloy or FeCrAl-clad fuel assemblies. The basic 18-month cycle length core was first designed with Zr alloy fuel then extended to 24-month cycle length core with FeCrAl-clad fuel. For the 18-month equilibrium cycle, the cycle length requirements are valued at 510 Effective Full Power Days (EFPDs) with ~30–45 days of outage and this corresponding value for the 24-month cycle with the same outages is 692 EFPDs.

Various constraints were placed on the core design variables during the optimization. The main constraint was the limit on the assembly design options specified by their fuel enrichments and burnable poison loading, including the IFBA and WABA. Different assembly options were tested for the 18-month Zr-clad core, the 18-month, and 24-month FeCrAl core to meet the energy production requirements, which is the main design objective.

Operational and safety constraints that must be satisfied during the optimization of the equilibrium cycle include reactivity and thermal limits that ensure reactor safety. Reactivity limits, which ensure negative feedback for temperature excursions, include a constraint that is the maximum soluble boron concentration. This constraint on the boron concentration is needed to control the axial offset due to boron deposition and maintain a negative temperature coefficient of reactivity throughout the lifetime of the core. As a high-soluble boron concentration is needed to control core reactivity and prevent high-power density regions in the core, burnable poisons are added to the core design to supplement reactivity control and maintain criticality. Hence, to prevent a positive moderator temperature coefficient, the threshold for the boron concentration is set at 1300 ppm for both 18 and 24-month core designs [36]. It is noted that for the extended burnup (24-month) core design, negative temperature coefficient was found in a limiting core design with threshold value of 1700 ppm [37].

Thermal limits are required to minimize radiological release during normal, transient, and accident conditions by maintaining fuel-cladding integrity. The thermal limits examined include the heat flux hot channel factor (or pin peaking factor), F_Q, and the enthalpy rise hot channel factor, $F_{\Delta H}$. F_Q is the ratio of

the peak pin power to the core average pin power and used to set the fuel centerline temperature to prevent fuel damage.

Table 2-3. Core design parameter limits.

Parameter	Limit
Heat flux hot channel factor (F_Q)	2.1
Enthalpy rise hot channel factor ($F_{\Delta H}$)	1.65
Peak pin burnup (GWD/MTU)	62
Peak boron concentration (ppm)	1300
Moderator temperature coefficient (pcm/K)	0.0

Table 2-3 summarizes main core design parameters and their limits. Typical F_Q limit used to set as 2.5 based on the large break LOCA (LBLOCA) analysis [38]. In this research, F_Q was set as 2.1 to give more conservative result. $F_{\Delta H}$ represents rod-integrated power thermal limit, which set a limit on the fuel-cladding critical heat flux to ensure the departure from nucleate boiling does not occur. In this research $F_{\Delta H}$ was set as 1.65, which is based on the previous safety evaluation of WBN-1 [38]. The rod-averaged discharge burnup limit was set as 62 GWD/MTU based on the current regulatory limit for the 18-month cycle. However, for the 24-month cycle which requires an extended burnup, the limit can be increased up to 75 or 80 GWD/MTU.

2.1.4 Reactivity Compensation for FeCrAl-Clad Fuel

The Zr alloy has very small thermal neutron absorption cross section (0.2 barn). The cross section of FeCrAl is ten times larger (2.43 barn), which leads to an increased parasitic absorption of neutrons in the FeCrAl cladding material when compared to Zr alloy clad. Figure 2-3 shows absorption cross section comparison between Zr alloy and FeCrAl [33].

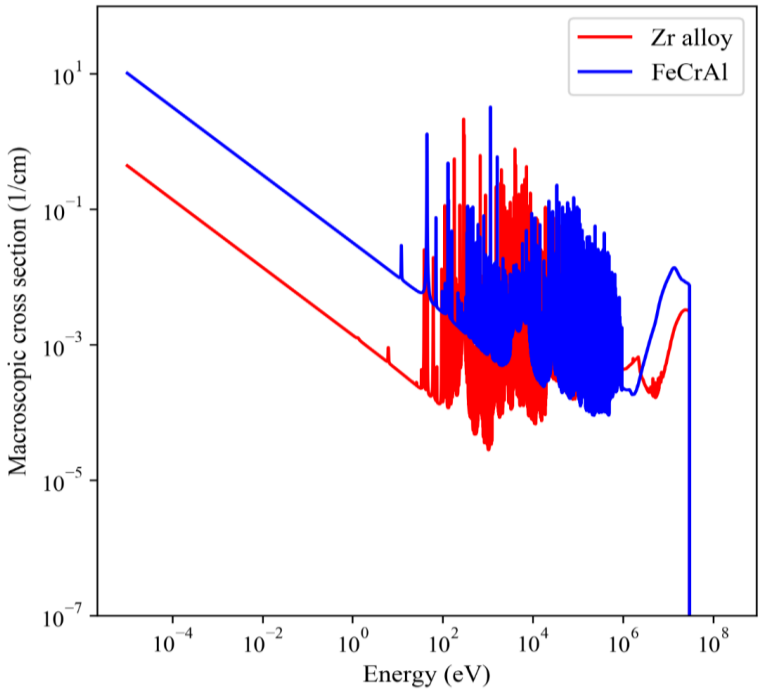

Figure 2-3. Neutron absorption cross section of Zr alloy and FeCrAl material [33].

This reactivity penalty inevitably leads to a shortened cycle length and as such, attempts are made to match the end-of-cycle (EOC) reactivity of the FeCrAl material with that of Zr alloy, thus maintaining the cycle energy production. The case study was performed for a fuel assembly design with the reference enrichment of 4.1% and 128-IFBA fuel pins. These cases include combination of different cladding thickness and enrichment.

Table 2-4 gives different cases used in this study to compensate for the neutron loss due to absorption. Case 1 attempted to address the issue by employing thinner FeCrAl cladding, and three thicknesses are considered, including 0.0422 cm, 0.0472 cm, and 0.0522 cm. The choice of cladding thickness is corroborated from the calculated minimum thickness of FeCrAl cladding based on elastic buckling and ovality [29]. Case 2 aims to enhance the initial reactivity by increasing the fuel enrichment and fuel pellet radius, while adopting the minimum allowable thickness of the FeCrAl cladding. Case 3 and 2 are similar; however, the fuel pellet radius is not maintained. Finally, Case 4 only attempts to increase the fresh fuel enrichment.

Table 2-4. Case studies to compensate FeCrAl reactivity penalty.

Case	Enrichment (wt.%)	Clad Thickness (cm)	Fuel Pellet Radius (cm)
1	4.10	0.0422–0.0522	0.4096
2	4.53	0.04	0.4268
3	4.70	0.04	0.4096
4	5.0	0.0572	0.4096

The comparison of the impact of the above cases on the multiplication factor (k_{inf}) curve is shown in Figure 2-4 which was performed by POLARIS code in SCALE [12].

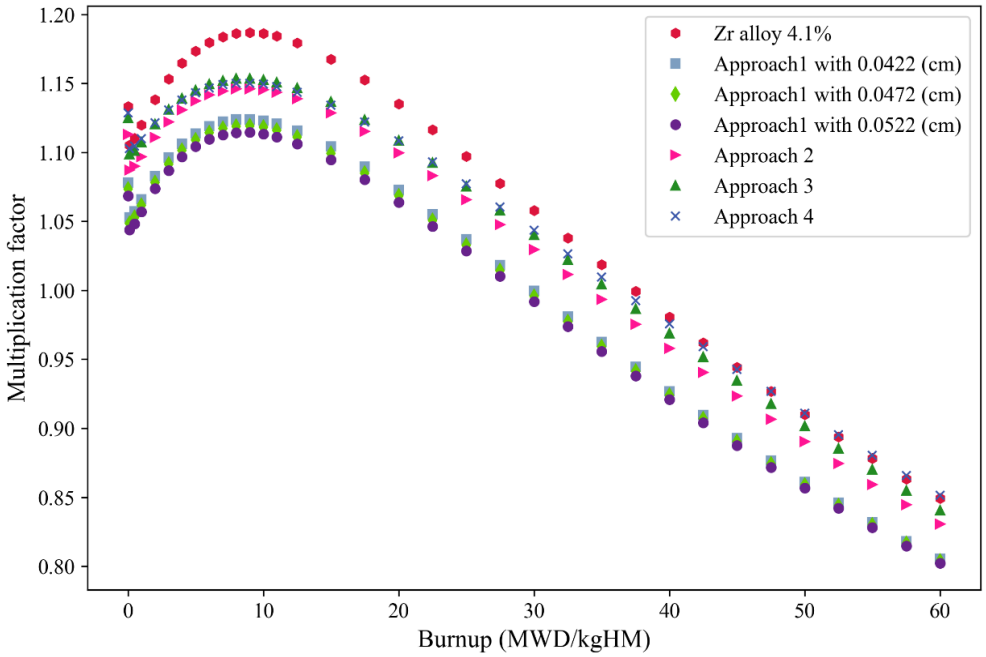

Figure 2-4. Comparison of the k_{inf} with and without ATF fuels.

Fuel pin nodalization includes 16 radial nodes and 8 azimuthal nodes. The ray spacing was set to 0.01 cm in the depletion calculation for more accurate IFBA pin modeling. It was observed that the effect of only decreasing cladding thickness (Case 1) is minimal in compensating the reactivity penalty, while Cases 2, 3, and 4 show significant effects in alleviating the k_{inf} penalty and matching the EOC reactivity to that of the non-ATF (i.e., Zr-clad fuel).

As a result of reactivity compensation study, Case 4 was selected for the further FeCrAl core design specification in this research. Since only the fuel enrichment is increased (from 4.1% to 5%) and the fuel rod geometry remains unchanged in Case 4, the core thermal-hydraulics characteristics are expected be consistent with the case where conventional Zr alloy cladding is used.

2.1.5 FeCrAl Fuel Assembly Design

The FeCrAl fuel assembly was designed with a slightly increased enrichment (with the same 128-IFBA loading). The enrichment was set as 4.5wt.% for Zr-clad fuel and 5.5wt.% for FeCrAl-clad fuel. Figure 2-5 shows the resulting k_{inf} curve of the two types of fuel assembly. Due to the increased enrichment of ^{235}U in the FeCrAl case, the burnable poison IFBA depleted much faster than in the reference model, resulting in a lower peak k_{inf} value. However, since the goal of the following core design optimization is to maintain the cycle length, this discrepancy could be neglected and focus on the reactivity at EOC, which shows fairly good agreement. These two case studies provide the guidance of fuel assembly design in the core design problem when FeCrAl is adopted as the cladding material.

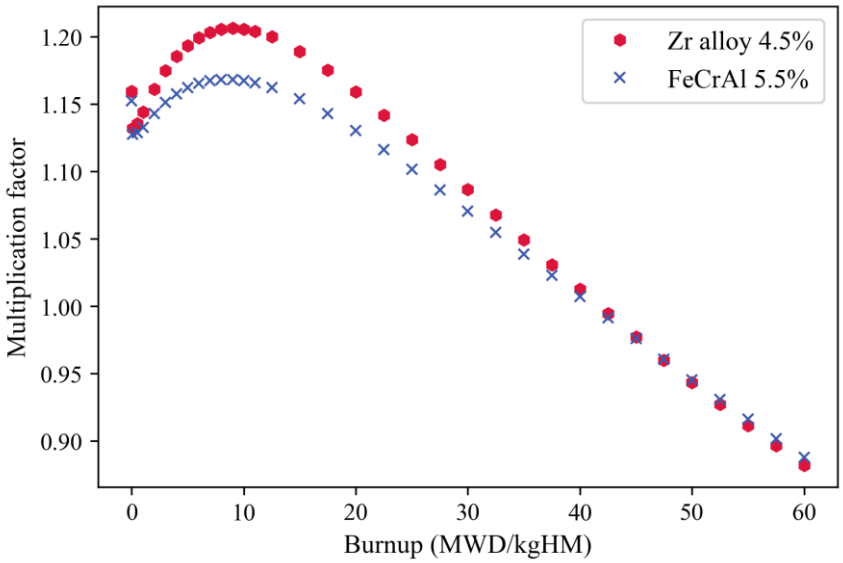

Figure 2-5. k_{inf} comparison between Zr-clad and FeCrAl-clad fuels by using POLARIS.

Figure 2-6 shows the isotopic concentrations of select isotopes ^{235}U, ^{238}U and ^{239}Pu. For better comparison in the plot, the concentrations of the ^{235}U and ^{239}Pu isotopes are increased by a factor of 100. Also evident in the plot is a higher concentration of ^{235}U in the FeCrAl-clad fuel as a direct consequence of the increased enrichment required to alleviate the neutronic penalty. However, the ^{239}Pu concentration in the FeCrAl-clad fuel is higher than Zr-clad fuel and this higher plutonium production compensates for the shortened cycle length associated with the use of FeCrAl-clad fuel.

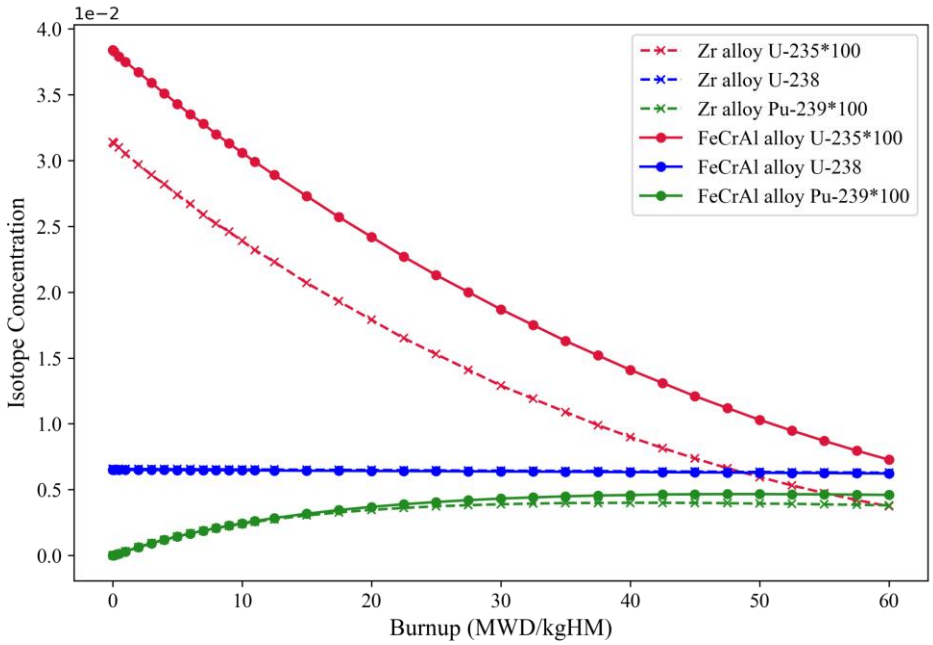

Figure 2-6. Isotopic concentration of select isotopes for the Zr-clad and FeCrAl-clad fuels.

2.2 FeCrAl PWR Equilibrium Cycle Development

The reactor core is loaded with 84 fresh fuel assemblies in a 3-region scheme, where each region is split into 2-batches. The equilibrium cycling scheme is presented in Table 2-5 with the lower and higher enrichments represented as batch "a" and "b," respectively.

Table 2-5. Equilibrium cycling scheme.

Cycle/Region	n	n+1	n+2	n+3
…	…	…	…	…
m/b	25	0	0	0
m+1/a	59	0	0	0
m+1/b	25	25	0	0
m+2/a	59	59	0	0
m+2/b	25	25	25	0
m+3/a	0	59	59	0
m+3/b	0	25	25	25
m+4/a	0	0	59	59
m+4/b	0	0	25	25
…	…	…	…	…

The simulation of the equilibrium cycle calculation was conducted using the high-fidelity multi-physics code simulation code VERA-CS. The "jump-in" technique was utilized to reduce the code execution time since VERA-CS simulation is computationally intensive due to the use of high-order transport methods to solve the 3D reactor core problem. In general, the individual fuel assembly results were used from the full-core simulation result of the previous cycle for jump-in core configuration. There are three basic steps required:

1. Perform single fuel assembly depletion calculations for each unique fuel assembly type for all previous cycles,
2. Perform a full-core fuel shuffling calculation using the results of the single fuel assembly depletion calculations,
3. Perform full-core depletion calculations to establish the equilibrium cycle.

Before exploring the possibility of creating a 24-month cycle with FeCrAl ATF loaded PWR equilibrium cycle, an 18-month cycle with Zr-clad fuel was first designed and tested. Then, 18-month cycle with FeCrAl-clad fuel core was developed and extended to 24-month cycle. Hence, following three equilibrium cycles were developed using VERA-CS:

- 18-month cycle with Zr-clad fuel core
- 18-month cycle with FeCrAl-clad fuel core
- 24-month cycle with FeCrAl-clad fuel core

and their core configurations and cycle performance are summarized below.

2.2.1 18-month Cycle with Zr-Clad Fuel Core

The cycle length requirements for the equilibrium cycle are 18 months, which is evaluated as 510 EFPD with 30–45 days for outages. Table 2-6 shows fuel assembly design specifications. Five different types of assemblies were used with different enrichment and IFBA and WABA burnable poison loading patterns.

Table 2-6. Assembly specification for 18-month Zr-clad fuel core.

Assembly ID	Enrichment (wt.%)	IFBA Rods	WABA Rods
TYPE01	4.1	104	0
TYPE02	4.1	128	0
TYPE03	4.5	16	0
TYPE04	4.5	128	0
TYPE05	4.5	128	24

Figure 2-7 is core configuration of 18-month with Zr-clad fuel core. Two batches, denoted as “a” and “b,” with three regions, fresh, once-, and twice-burned, are combined. The core follows a low-leakage loading pattern (i.e., L^3P) with the burned assemblies at the periphery of the core.

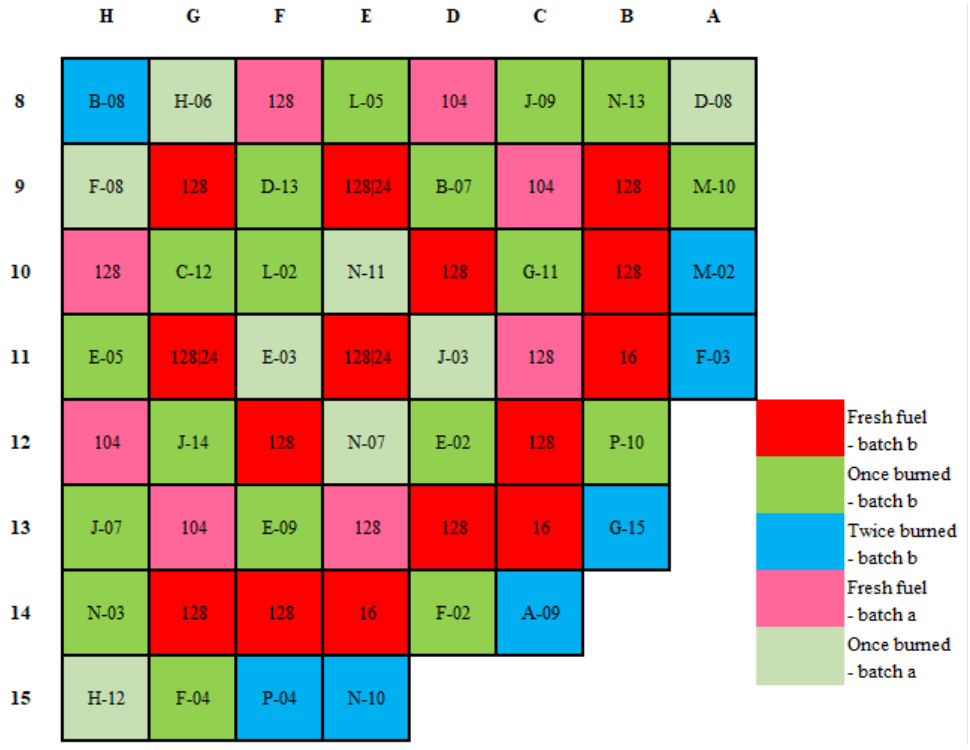

Figure 2-7. Core configuration and loading pattern of the 18-month Zr-clad fuel core.

Table 2-7 shows the key cycle performance parameters of this equilibrium core. The 18-month cycle is equivalent to 510.4 EFPD. The value of $F_{\Delta H}$ and F_Q is 1.471 and 1.75, both well below the limits. The

moderator temperature coefficient is negative throughout the cycle with the peak value being -13.19 pcm/K. In general, all operational, thermal, and safety limits are satisfied.

Table 2-7. Equilibrium cycle parameters of the 18-month Zr-clad fuel core.

Parameters	Value
Cycle burnup (GWD/MTU)	19.603
Cycle length (EFPD)	510.4
Peak pin burnup (GWD/MTU)	57.95
Peak assembly burnup (GWD/MTU)	55.57
Peak boron concentration (ppm)	1293
Enthalpy rise hot channel factor ($F_{\Delta H}$)	1.471
Heat flux hot channel factor (F_Q)	1.75
Moderator temperature coefficient (pcm/K)	-13.19

Figure 2-8 and Figure 2-9 show relative assembly power at BOC and EOC, respectively. The results indicate the highest power densities are observed in the TYPE01 assemblies with lowest enrichment and burnable poison values at BOC. This trend changes as the cycle progresses from BOC to EOC, as the higher enrichment assemblies in the central area of the core dominate in power densities. The assembly averaged burnup distribution is depicted in Figure 2-10 and Figure 2-11, respectively, at BOC and EOC.

	H-	G-	F-	E-	D-	C-	B-	A-
8	0.92	1.08	1.21	1.21	1.34	1.25	1.04	0.49
9	1.08	1.26	1.16	1.04	1.26	1.33	1.10	0.51
10	1.21	1.15	1.14	1.04	1.28	1.25	1.09	0.43
11	1.21	1.04	1.03	0.96	1.06	1.22	1.17	0.32
12	1.34	1.25	1.27	1.05	1.15	1.17	0.71	
13	1.25	1.32	1.24	1.20	1.16	1.08	0.37	
14	1.04	1.09	1.08	1.15	0.70	0.37		
15	0.49	0.50	0.43	0.32				

Figure 2-8. 2D BOC power distribution of Zr-clad fuel core (ratio of assembly/core average assembly power).

	H-	G-	F-	E-	D-	C-	B-	A-
8	0.87	1.00	1.27	1.15	1.27	1.06	0.97	0.54
9	1.00	1.27	1.09	1.27	1.12	1.26	1.17	0.58
10	1.27	1.09	1.06	1.04	1.30	1.11	1.16	0.50
11	1.15	1.27	1.04	1.23	1.03	1.24	1.05	0.36
12	1.27	1.12	1.30	1.02	1.07	1.21	0.70	
13	1.06	1.26	1.11	1.24	1.20	1.00	0.40	
14	0.97	1.17	1.16	1.06	0.70	0.40		
15	0.54	0.58	0.50	0.36				

Figure 2-9. 2D EOC power distribution of Zr-clad fuel core (ratio of assembly/core average assembly power).

	H-	G-	F-	E-	D-	C-	B-	A-
8	38.99	24.85	0.00	21.78	0.00	24.80	19.63	26.29
9	24.85	0.00	23.58	0.00	22.90	0.00	0.00	26.03
10	0.00	23.73	21.24	24.82	0.00	23.19	0.00	35.96
11	21.78	0.00	24.98	0.00	26.15	0.00	0.00	46.35
12	0.00	23.07	0.00	26.25	21.32	0.00	22.67	
13	24.80	0.00	23.27	0.00	0.00	0.00	36.42	
14	19.63	0.00	0.00	0.00	22.76	36.39		
15	26.29	26.14	35.93	46.33				

Figure 2-10. 2D BOC burnup distribution of Zr-clad fuel core (GWD/MTU).

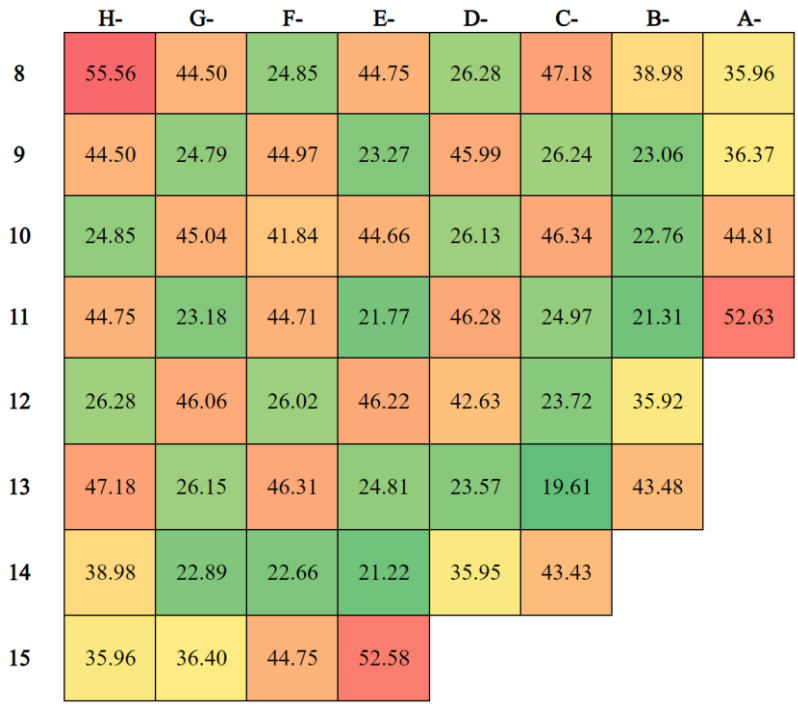

Figure 2-11. 2D EOC burnup distribution of Zr-clad fuel core (GWD/MTU).

2.2.2 18-Month Cycle with FeCrAl-Clad Fuel Core

Similar to 18-month cycle with Zr-clad fuel core design, five different types of assemblies were used with different enrichment and IFBA and WABA burnable poison loading patterns. Table 2-8 shows fuel assembly design specifications of 18-month cycle with FeCrAl-clad fuel core. To compensate neutron penalty of FeCrAl-clad fuel, enrichment of batches “a” and “b” were increased to 5.2 wt.% and 5.7 wt.%, respectively.

Table 2-8. Assembly specification for the 18-month FeCrAl-clad fuel core.

Assembly ID	Enrichment (wt.%)	IFBA Rods	WABA Rods
TYPE01	5.2	104	0
TYPE02	5.2	200	0
TYPE03	5.7	200	0
TYPE04	5.7	128	0
TYPE05	5.7	128	24

Figure 2-12 is core configuration of 18 months with FeCrAl-clad fuel core. Two-batches, “a” and “b,” with three regions, fresh, once-, and twice-burned, are combined. The core follows a low-leakage loading pattern (i.e., L^3P) with the burned assemblies at the periphery of the core.

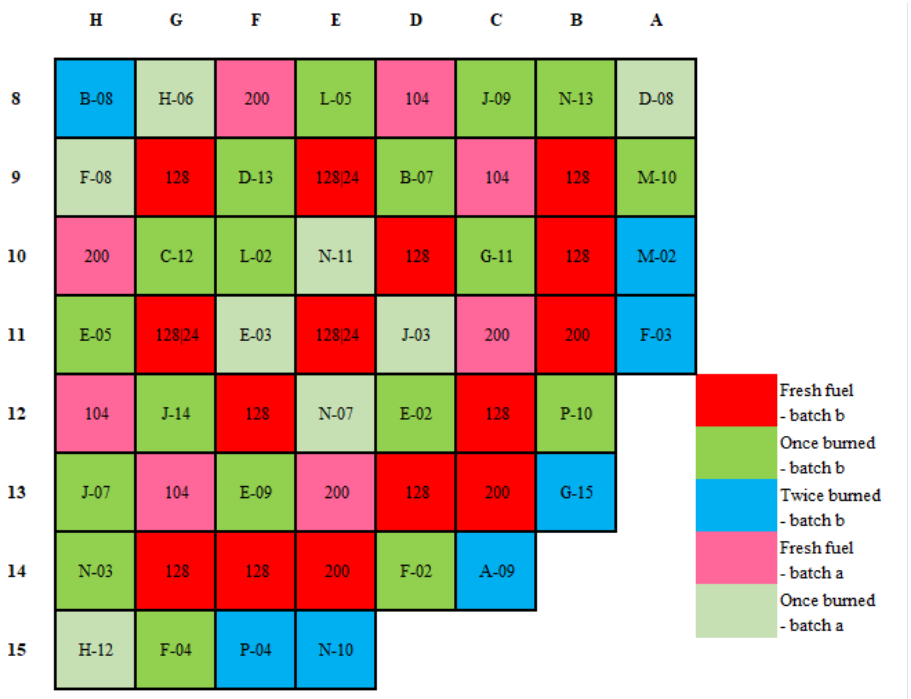

Figure 2-12. Core configuration and loading pattern of the 18-month FeCrAl-clad fuel core.

Table 2-9 shows the key parameters of the 18-month FeCrAl-clad fuel core equilibrium cycle. The parameters satisfy the requirement of both safety and thermal limit. It can be observed that the values for operational and thermal limits are higher than those of the 18-month Zr-clad fuel core design, although sufficient margins are maintained from the limit.

Table 2-9. Equilibrium cycle performance for the 18-month FeCrAl-clad core design.

Core Parameters	Value
Cycle burnup (GWD/MTU)	19.596
Cycle length (EFPD)	510.2
Peak pin burnup (GWD/MTU)	58.56
Peak assembly burnup (GWD/MTU)	55.31
Peak boron concentration (ppm)	1298
Enthalpy rise hot channel factor ($F_{\Delta H}$)	1.621
Heat flux hot channel factor (F_Q)	1.92
Moderator temperature coefficient (pcm/K)	-13.88

Figure 2-13 and Figure 2-14 show relative assembly power at BOC and EOC, calculated from VERA-CS. The results are similar to the results observed above for the Zr-clad core design with the changes observed as a result of the changes in the core design and assembly options. The assembly averaged burnup distribution at BOC and EOC is depicted in Figure 2-15 and Figure 2-16, respectively.

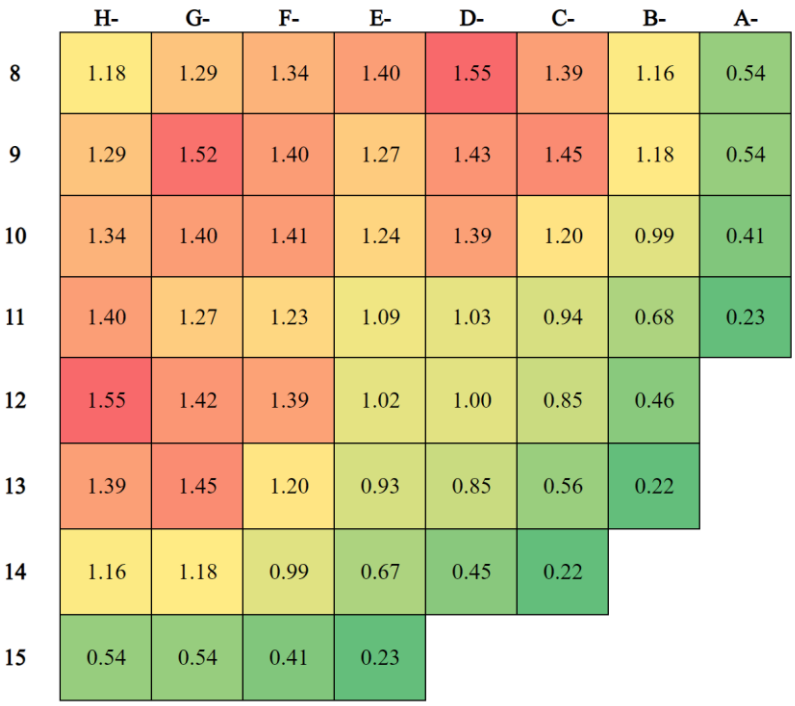

Figure 2-13. 2D BOC power distribution of 18-month FeCrAl-clad fuel core (ratio of assembly/core average assembly power).

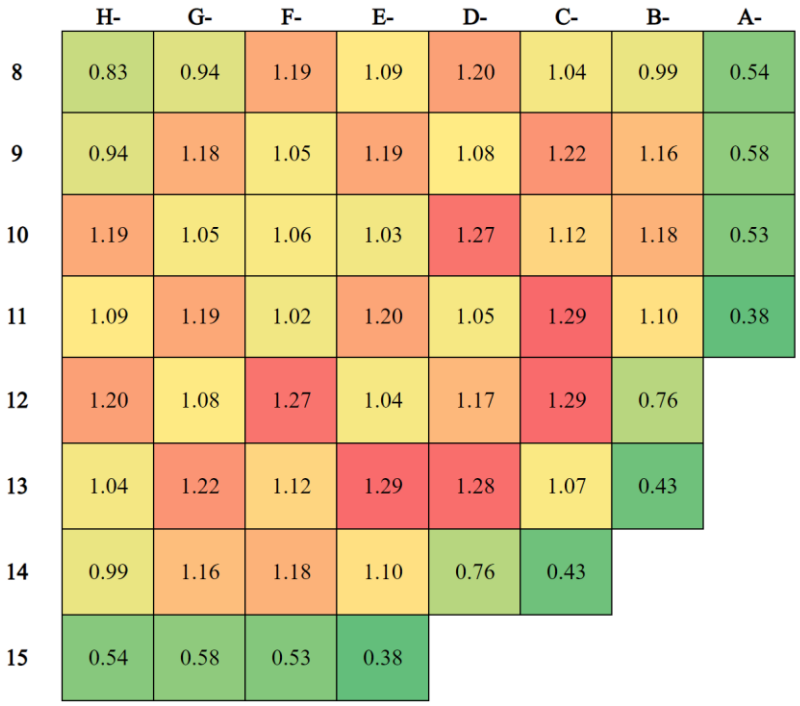

Figure 2-14. 2D EOC power distribution of 18-month FeCrAl-clad fuel core (ratio of assembly/core average assembly power).

	H-	G-	F-	E-	D-	C-	B-	A-
8	37.04	25.12	0.00	22.54	0.00	25.88	16.40	26.76
9	25.12	0.00	21.92	0.00	23.12	0.00	0.00	26.37
10	0.00	22.06	18.06	22.98	0.00	24.14	0.00	34.03
11	22.54	0.00	23.12	0.00	26.35	0.00	0.00	47.00
12	0.00	23.25	0.00	26.42	18.15	0.00	21.81	
13	25.88	0.00	24.20	0.00	0.00	0.00	37.08	
14	16.40	0.00	0.00	0.00	21.90	37.06		
15	26.76	26.46	34.00	46.96				

Figure 2-15. 2D BOC burnup distribution of 18-month FeCrAl-clad fuel core (GWD/MTU).

	H-	G-	F-	E-	D-	C-	B-	A-
8	55.32	45.86	25.12	46.29	26.75	48.88	37.04	36.88
9	45.86	25.87	45.02	24.20	47.02	26.42	23.25	37.07
10	25.12	45.09	40.99	44.46	26.46	47.00	21.90	43.08
11	46.29	24.14	44.52	22.54	46.74	23.12	18.15	52.81
12	26.75	47.09	26.37	46.69	39.86	22.06	34.01	
13	48.88	26.35	46.96	22.98	21.92	16.40	43.44	
14	37.04	23.11	21.81	18.06	34.03	43.40		
15	36.88	37.09	43.02	52.75				

Figure 2-16. 2D EOC burnup distribution of 18-month FeCrAl-clad fuel core (GWD/MTU).

2.2.3 24-Month Cycle with FeCrAl-Clad Fuel Core

For the 24-month cycle, the total EFPD is estimated as 692 with 30-45 days of reloading period. The challenge of achieving an optimized core design filled with FeCrAl-clad fuel is that the increase in fuel

enrichment required to reach a high level of burnup, however, this will cause an excessively large reactivity at BOC. As a result, a large amount of soluble boron is necessary at BOC, which may impose challenges in maintaining a non-positive moderator temperature coefficient. Therefore, in order to keep the same 1300 ppm limit for the critical boron concentration, gadolinium (Gd) burnable poison was chosen for this core design to further offset the influence of the initial reactivity needed to drive the cycle length to the 24-month cycle length. Table 2-10 shows fuel assembly design specifications and amount of 24-month cycle with FeCrAl-clad fuel core.

Table 2-10. Assembly specification for the 24-month FeCrAl core fuel core.

Assembly ID	Enrichment (wt.%)	IFBA Rods	WABA Rods	Assemblies
TYPE01	7.25	200	0	4
TYPE02	5.075	200	16	4
TYPE03	7.25	200	4	20
TYPE04	5.425	200	16	32
TYPE05	7.75	200	4	24

Similar to 18-month cases, five different types of assemblies were used with different enrichment, IFBA and gadolinium burnable poison loading. Two Gd loadings were considered in fuel assembly TYPE02-05, including 16 rods with 6% Gd concentration in the fuel matrix and 4 rods with a 2% concentration. The element was assumed to be enriched to 100% ^{157}Gd enrichment in both loading designs.

Figure 2-17 shows core design for FeCrAl-clad fuel loaded PWR 24-month cycle. Two batches ("a" and "b") with three regions, fresh, once-, and twice-burned, are combined. The core follows L^{3}P with the burned assemblies at the periphery of the core.

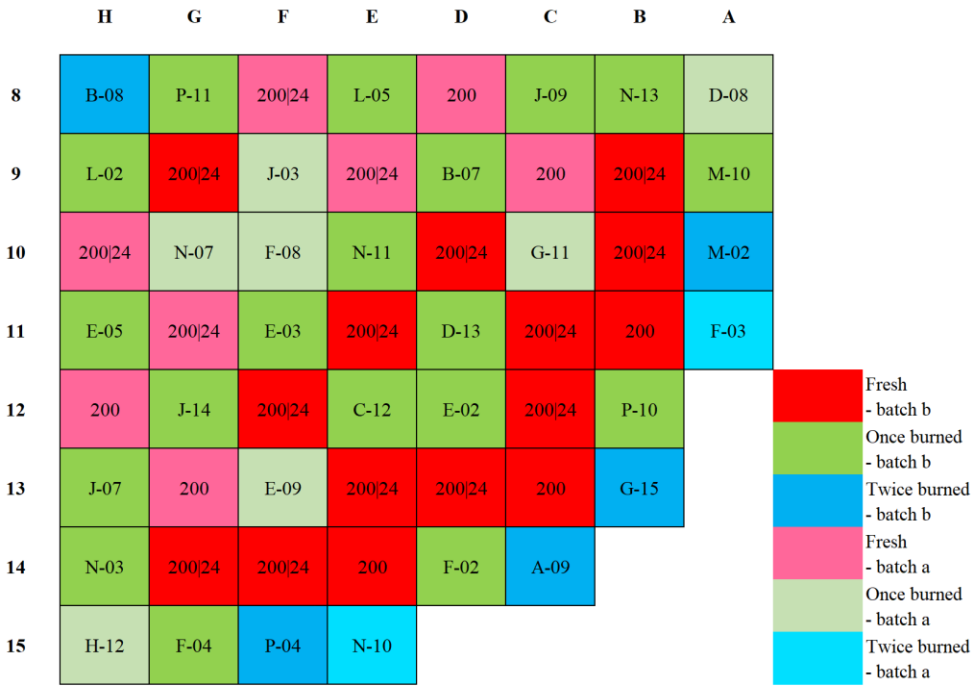

Figure 2-17. Core configuration and loading pattern of the 24-month FeCrAl-clad fuel core.

The equilibrium cycle performance is summarized in Table 2-11.

Table 2-11. Equilibrium cycle performance for the 24-month FeCrAl-clad core design.

Core Parameters	Value
Cycle burnup (GWD/MTU)	26.840
Cycle length (EFPD)	697.4
Peak pin burnup (GWD/MTU)	81.87
Peak assembly burnup (GWD/MTU)	77.85
Peak boron concentration (ppm)	1281
Enthalpy rise hot channel factor ($F_{\Delta H}$)	1.614
Heat flux hot channel factor (F_Q)	2.05
Moderator temperature coefficient (pcm/K)	-17.28

The cycle length was slightly extended than initial design of 692 EFPD. This is achieved mainly because of the high fuel burnup with the peak rod discharge burnup was set to 82 GWd/MTU. Both safety and thermal limits were also satisfied throughout the cycle, though the peak critical boron concentration has been further reduced to the limits 1300 ppm that is typical for the 18-month cycle. The results were obtained from numerous assemblies containing burnable poisons were used in the core design. The 1300 ppm limit was enforced in the extended burnup design as an important parameter in coolant chemistry and to retain negative temperature feedback effect during the operation.

The core radial power distribution at BOC and EOC is shown in Figure 2-18 and Figure 2-19, respectively. The slight asymmetry was observed in the EOC power distribution are a result of the arrangement of higher enriched fuel assemblies in those locations following the depletion of the burnable poisons. Figure 2-20 and Figure 2-21 show burnup distribution of the updated 24-month FeCrAl-clad fuel core at BOC and EOC, respectively. The distribution is similar to the 18-month FeCrAl-clad core design with increased burnup values observed for this core design.

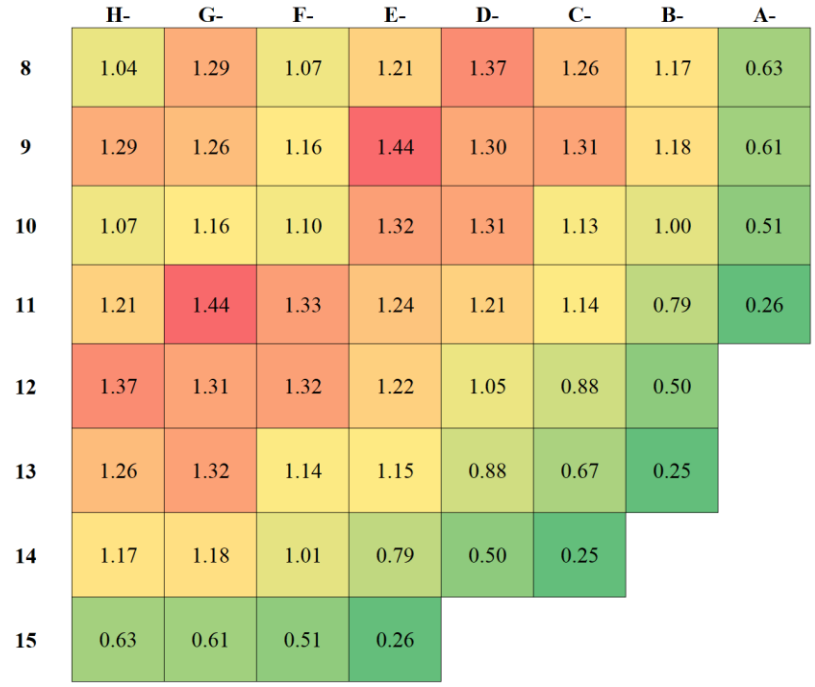

	H-	G-	F-	E-	D-	C-	B-	A-
8	1.04	1.29	1.07	1.21	1.37	1.26	1.17	0.63
9	1.29	1.26	1.16	1.44	1.30	1.31	1.18	0.61
10	1.07	1.16	1.10	1.32	1.31	1.13	1.00	0.51
11	1.21	1.44	1.33	1.24	1.21	1.14	0.79	0.26
12	1.37	1.31	1.32	1.22	1.05	0.88	0.50	
13	1.26	1.32	1.14	1.15	0.88	0.67	0.25	
14	1.17	1.18	1.01	0.79	0.50	0.25		
15	0.63	0.61	0.51	0.26				

Figure 2-18. 2D BOC power distribution of the 24-month FeCrAl-clad fuel core (ratio of assembly/core average assembly power).

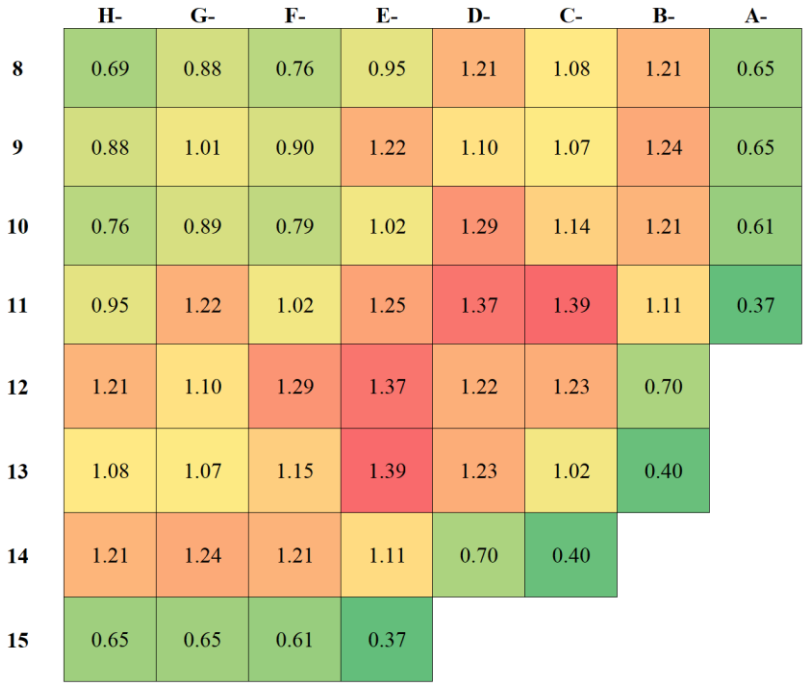

	H-	G-	F-	E-	D-	C-	B-	A-
8	0.69	0.88	0.76	0.95	1.21	1.08	1.21	0.65
9	0.88	1.01	0.90	1.22	1.10	1.07	1.24	0.65
10	0.76	0.89	0.79	1.02	1.29	1.14	1.21	0.61
11	0.95	1.22	1.02	1.25	1.37	1.39	1.11	0.37
12	1.21	1.10	1.29	1.37	1.22	1.23	0.70	
13	1.08	1.07	1.15	1.39	1.23	1.02	0.40	
14	1.21	1.24	1.21	1.11	0.70	0.40		
15	0.65	0.65	0.61	0.37				

Figure 2-19. 2D EOC power distribution of the 24-month FeCrAl-clad fuel core (ratio of assembly/core average assembly power).

	H-	G-	F-	E-	D-	C-	B-	A-
8	58.44	24.54	50.14	34.66	0.00	33.31	0.00	32.90
9	24.54	0.00	37.03	0.00	30.90	27.64	0.00	31.57
10	50.14	37.03	48.95	33.56	0.00	35.67	0.00	33.98
11	34.66	0.00	33.57	0.00	0.00	0.00	0.00	63.52
12	0.00	30.86	0.00	0.00	26.58	0.00	37.17	
13	33.31	27.52	35.51	0.00	0.00	0.00	48.68	
14	0.00	0.00	0.00	0.00	37.05	48.79		
15	32.90	31.43	33.95	63.52				

Figure 2-20. 2D BOC burnup distribution of the 24-month FeCrAl-clad fuel core (GWD/MTU).

	H-	G-	F-	E-	D-	C-	B-	A-
8	77.55	48.95	71.35	61.48	33.31	63.39	32.93	50.15
9	48.95	26.58	61.37	33.95	61.49	58.44	33.57	48.79
10	71.35	61.34	71.77	63.48	35.50	66.38	31.43	49.52
11	61.48	33.98	63.52	34.66	36.97	37.05	27.52	72.28
12	33.31	61.56	35.67	37.03	58.87	30.86	54.37	
13	63.39	58.42	66.48	37.17	30.90	24.54	57.89	
14	32.93	33.56	31.56	27.64	54.32	58.01		
15	50.15	48.68	49.55	72.36				

Figure 2-21. 2D EOC burnup distribution for the 24-month FeCrAl-clad fuel core (GWD/MTU).

3. SEVERE ACCIDENT ANALYSIS

3.1 Summary of Accident Scenario Analysis Method

A LBLOCA in a typical Westinghouse 4-loop PWR is analyzed in MELCOR with the ECCS automatic actuation assumed to fail. Analysis was performed for the conventional Zr-clad fuel and FeCrAl-clad fuel and key simulations outputs were investigated, including water level, system pressure, fuel/cladding temperature, hydrogen generation, time of gap release, and fission product release fraction. A model of the Zion nuclear power station, originally developed by Brookhaven National Laboratory and subsequently modified by Sandia National Laboratories, was utilized as a starting point [39]. The transient is initiated by a double-ended guillotine rupture of the pressurizer loop at the reactor coolant pump inlet and the reactor is assumed to scram. The model was developed to support the calculation of the source term for recovered LOCAs. As such, the LPSI system, which is initially assumed to fail, was assumed to be recovered (i.e., by manual startup) by operators 27 minutes after reactor scram. This case is of a particular interest with FeCrAl-clad, as this has the potential to delay (although not ultimately prevent) the onset of core melt, hence reducing the fission product release; therefore, reducing the source terms in recovered LOCAs.

Two steps of analysis were performed:

- Perform a complementary analysis based on the reference [6] for a LBLOCA with recovery of the LPSI system using the latest capabilities of MELCOR and, therefore, develop a capability to further analyze such transients for high burnup and/or uprated fuels. Notably, this enables source term analysis through modeling of radionuclide transport and, ultimately, consequence analysis through coupling to MACCS code in the future research. This supports quantification of the source term and, consequently, the recovered margin with FeCrAl cladding compared to Zr cladding.
- Analyze the sensitivity of coping time to burnup and core operating time and investigate the potential for utilizing the recovered margin to extend burnup and/or cycle length within current safety limits.

3.2 Modeling of Zion PWR

The Zion NPP was built on the shore of Lake Michigan in Zion, Illinois, and operated from 1973 until 1998 [41]. The plant consisted of two Westinghouse four-loop PWR units that each provided 1040 MWe for the Chicago area. Further details on the Zion reactor are provided below in Table 3-1.

A legacy MELCOR input of the Zion reactor was provided by SNL and the U.S. NRC. This MELCOR model has been used previously to support NRC evaluations of radiological consequences of design basis accidents using the revised source term [43] and [44]. The model simulates a LBLOCA, specifically a double-ended guillotine rupture of the pump suction piping. In this scenario, the LBLOCA event is followed by an initial failure of the LPSI system of ECCS due to equipment failure. However, unlike the previous LOCA analysis of the Surry reactor [45] and [46] the LPSI capability is restored shortly after the reactor water levels fall below the bottom of active fuel which occurs 27 minutes after the onset of the LOCA event an assumption of this research [39].

The SNL/NRC Zion model was originally based on an input from Brookhaven National Laboratory, before being modified at SNL for use in MELCOR Versions 1.8.4 and 1.8.5. The accident scenario and nodalization were edited by Texas A&M for station black-out comparisons with finely nodalized MAAP4 and SCDAP/RELAP5 calculations [44], before the input was converted from Version 1.8.6 to 2.0 by the Nuclear Safety Institute, IBRAE. This MELCOR 2.0 input was then converted back to the LBLOCA accident scenario [47]. The results from this most recent Version 2.0 LBLOCA model predicted limited core damage during the time when the core is uncovered, which is arrested by core reflooding after the reactivation of the LPSI system [48].

Table 3-1. Zion reactor core description [42].

Parameter	Value
Reactor thermal power (MWth)	3250
Reactor electric power (Mwe)	1040
Number of fuel assemblies	193
Number of rod clusters	53 full-length 8 part-length
Fuel pin lattice	15x15
Assembly pitch (cm)	1.43
Number of fuel rods per assembly	204
Number of guide tubes per assembly	20
Number of instrumentation sheaths per assembly	1
Fuel material	UO_2
Fuel density (g/cm^3)	10.42
Fuel enrichment (wt.%)	2.248 − 3.292
Cladding material	Zircaloy-4
Cladding density (g/cm^3)	6.55
Control rod material	Ag-In-Cd
Control absorber density (g/cm^3)	10.17

In this work, the MELCOR 2.0 Zion LBLOCA input deck was modified for the newer MELCOR Version 2.2, Build 20234. The main relevant differences between MELCOR 2.0 and 2.2 are the corrections to the eutectics model method, the addition of a user-defined material capability, and improvements to the modeling of ATFs with extended options for oxidation definition [49]. The following subsections describe the modeling details.

3.2.1 Reactor Core Geometry

The NRC MELCOR model of the Zion reactor used the original 15×15 fuel pin lattice and Zircaloy cladding, with the gas gap smeared into the cladding region. The core geometry was updated to a 17×17 lattice using data from legacy fuel performance reports [50]. Two new models were created: Zr 17×17 and FeCrAl 17×17. The fuel geometry is presented in Table 3-2, with the MELCOR radial and axial nodalization schemes shown in Table 3-3 and Figure 3-1. Note that, for the original 15×15 model, the fuel-clad gap was smeared into the cladding material and not modeled as a separate region. The fuel pin surface areas, UO_2 fuel masses, and inter-pin flow areas were recalculated using the new 17×17 clad outer radius. The cladding masses were recalculated for the Zr model using the new geometry and the FeCrAl model using the new geometry and the FeCrAl density described in the following section.

Table 3-2. Fuel geometric parameter comparison between 15x15 and 17x17 assemblies.

Parameter	15×15	17×17
Fuel pin radius (m)	4.647×10^{-3}	4.095×10^{-3}
Fuel-clad gap thickness (m)	0.000×10^{-3}	8.500×10^{-5}
Cladding inner radius (m)	4.646×10^{-3}	4.180×10^{-3}
Cladding outer radius (m)	5.359×10^{-3}	4.750×10^{-3}

Table 3-3. Axial and radial nodes parameters.

Axial Nodes			Radial Nodes		
Node ID	Lower Elevation (m)	Node Height (m)	Node ID	Ring Radius (m)	Number of Assemblies
Z1	0.1445	0.5511	R1	0.4362	13
Z2	0.6956	0.4594	R2	0.9133	44
Z3	1.1550	0.5585	R3	1.2396	44
Z4	1.7135	0.5230	R4	1.4767	48
Z5	2.2365	0.5230	R5	1.8800	44
Z6	2.7595	0.0508	R6	2.1970	0
Z7	2.8103	0.3048			
Z8	3.1151	0.3048			
Z9	3.4199	0.3048			
Z10	3.7247	0.3048			
Z11	4.0295	0.3048			
Z12	4.3343	0.3048			
Z13	4.6391	0.3048			
Z14	4.9439	0.3048			
Z15	5.2487	0.3048			
Z16	5.5535	0.3048			
Z17	5.8583	0.3048			
Z18	6.1631	0.3048			
Z19	6.4679	0.1698			

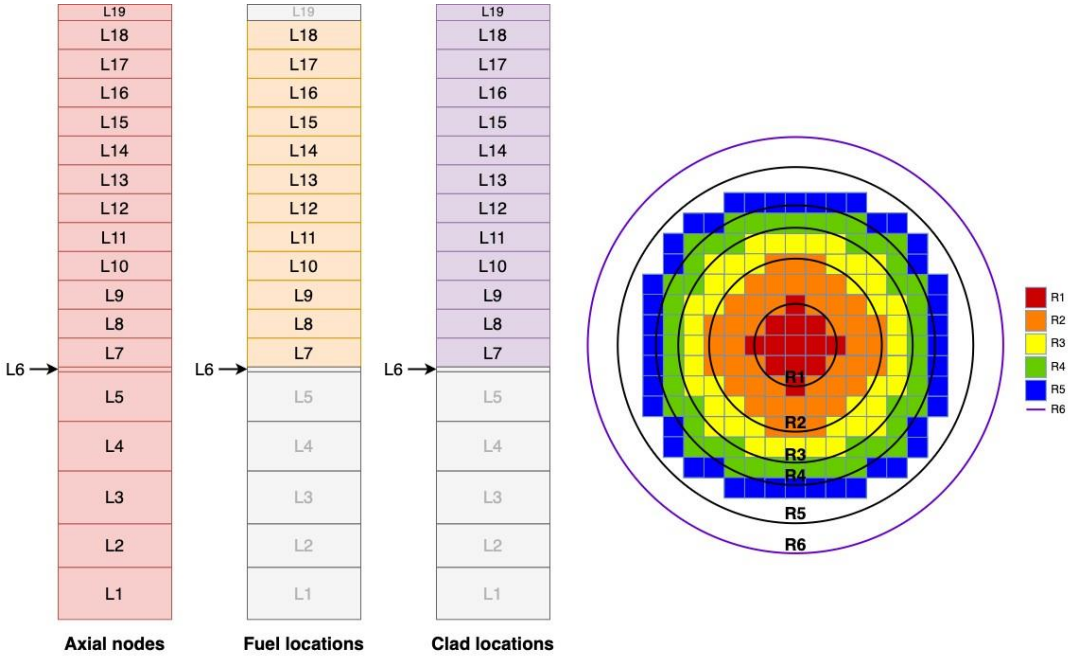

Figure 3-1. Axial and radial nodes for MELCOR modeling.

3.2.2 FeCrAl and FeCrAl Oxide Definition

Work on modeling FeCrAl-clad fuel using MELCOR version 1.86 has been already completed [51] and [52]. However, due to significant differences in modeling approach between MELCOR 1.86 and MELCOR 2.2, many of the methods developed in this previous work were not suitable for a direct application in the NRC Zion model for this study. This study, therefore, used MELCOR 2.2.

MELCOR 2.2 contains the new capability to create User-Defined Materials (UDMs) that allow the explicit definition of additional, non-default materials in MELCOR [53] and [54]. This new capability is used in this work to define the FeCrAl cladding material and FeCrAl oxide cladding material.

3.2.3 Material Properties

Table 3-4 summarizes material properties of FeCrAl and FeCrAl oxide.

3.2.3.1 Dynamic Viscosity

Dynamic viscosity information is required in MELCOR when a material becomes molten. MELCOR requires the dynamic viscosity and thermal expansivity for a metal to be input directly. The dynamic viscosity μ_i of an oxide material i is calculated using the empirical coefficients $ALPHI$ and in an Arrhenius form:

$$\mu_i = OXMUI \cdot \exp\left(\frac{ALPHI}{T}\right) \quad (1)$$

Due to the lack of available data for these parameters for FeCrAl and FeCrAl oxide, the default MELCOR values for stainless steel have been used. The dynamic viscosity required for FeCrAl was calculated using the FCA melting temperature of 1773 K and the stainless-steel defaults given in the MELCOR User Guide to solve Equation (1).

Table 3-4. Material properties of FeCrAl and FeCrAl oxide.

Parameter	FeCrAl	FeCrAl Oxide	Reference and Notes
Density (kg/m^3)	7100	5180	[32][56]
Melting point (K)	1773	1901	[32] [56]
Latent heat of fusion (J/kg)	270,000	687,463	[53]
Dynamic viscosity (Pa·s)	6.972×10^{-3}	-	Default for steel [53][[54]
Thermal expansivity per mol. vol. ($K^{-1}\cdot cm^{-3}$)	-	2.387×10^{-4}	Default for steel [53][[54]
$ALPHI$ (Eq. 1) (K^{-1})	-	3313	Default for steel [53][[54]
$OXMUI$ (Eq. 1) (Pa·s)	-	1.076×10^{-3}	Default for steel [53][[54]
Emissivity bounds	0.0~0.7	0.0~0.7	[57]
A (Eq. 2)	4.200×10^{-2}	0.7	FeCrAl/FeCrAl oxide example [53][[54]
B (Eq. 2)	3.474×10^{-4}	0.0	FeCrAl/FeCrAl oxide example [53][[54]

3.2.3.2 Emissivity

For a linear relation the emissivity, ϵ is calculated in MELCOR using the zero-temperature emissivity, A, and the emissivity gradient, B:

$$\epsilon = A + BT \tag{2}$$

There is a lack of exact data for FeCrAl and FeCrAl oxide emissivity, but the Kanthal APMT datasheet gives the maximum bound as 0.7 [57]. This is taken as the upper bound of the FeCrAl emissivity, with the rest of the data taken from the MELCOR User Guide FeCrAl/FeCrAl oxide example [53][54]. This is deemed acceptable given that previous work has used the same emissivity relation for FeCrAl/FeCrAl oxide as Zr/ZrO, changing only the maximum emissivity bound from 1.0 to 0.7 [58], and that sensitivity studies into varying emissivity parameters have found a negligible effect on heat transfer [59].

3.2.3.3 Temperature-dependent Properties

The FeCrAl and FeCrAl oxide specific heat, enthalpy, and thermal conductivity data are taken from a combination of the ORNL handbooks on FeCrAl [32]. The graphs are extrapolated to 2000 K, then held constant at any higher temperatures reached.

3.2.4 Oxidation Reactions

For alloys, MELCOR UDMs allow the definition of separate oxidation reactions for each component of the material. This is particularly useful for FeCrAl modeling due to the different oxidation behaviors of the component elements. As noted in previous section, FeCrAl cladding preferentially oxidizes Al_2O_3 below 1773 K to form a protective outer layer. Previous work without the UDM capability has been required to simplify this effect by considering the oxidation rate of the cladding as a whole rather than on an elemental basis [32] [60]. The UDM model enables these separate reactions to be explicitly included in the calculation. The oxidation reactions for FeCrAl cladding are defined in Equations (3–5).

$$Fe + H_2O \rightarrow FeO + H_2 + Q_{ox} \tag{3}$$

$Cr + 1.5\ H_2O \rightarrow 0.5\ Cr_2O_3 + 1.5\ H_2 + Q_{ox}$ (4)

$Al + 1.5\ H_2O \rightarrow 0.5\ Al_2O_3 + 1.5\ H_2 + Q_{ox}$ (5)

Once these chemical equations are defined, the oxidation rate coefficients for each element are then specified. These follow the parabolic rate equation described by Equation (6).

$$k_P = k_0 \exp\left(-\frac{E_a}{RT}\right) \quad (6)$$

where k_P is the reaction rate constant with respect to the metal reacted, k_0 is the mass gain rate constant, E_a is the activation energy, and R is the gas constant, and T is the temperature.

FeCrAl exhibits a breakaway oxidation reaction due to the protective layer of Al_2O_3 forming below 1773 K, resulting in a change in reaction behavior that is modeled using two different temperature ranges for Equation (6). Below 1773 K, the FeCrAl oxidation rate is modeled [62], and above 1773 K the default oxidation data for stainless steel is used as once the Al_2O_3 shell fails, FeCrAl oxidation is dominated by FeO in the same manner as stainless steel. This approach has been widely used in past analysis with good results [58][60][62].

These oxidation relations are shown in Table 3-5. Note that the oxidation reaction for FCA begins at 1323 K while MELCOR requires data from 1100 K, so the mass gain rate constant at the lower temperatures is set to zero. It should be noted that the mass gain constant, k_0, used in the literature is defined as the mass of oxide produced, whereas MELCOR requires the mass of metal reacted for each oxidation reaction. The data in Table 3-5 must be converted into metal mass and the individual elemental contribution found by taking the ratio of each metal present in FeCrAl.

Table 3-5. Oxidation equation coefficients.

Material	Temperature Range (K)	k_0 (g/cm^{2}s$^{0.5}$)	E_a (kJ/mol)	References and Notes
Zircaloy	1100−1850	5.44×10^{-1}	139	[63][54]
	1873−9900	9.39×10^{-1}	138	[63][54]
FeCrAl	1100−1323	0.00	344	-
	1323−1773	7.84	344	[64][68][11]
	1773−9900	2.40×10^{6}	352	[64][65]

3.2.5 Cladding Failure Modeling

MELCOR includes a detailed modeling of Zr-clad failure mechanisms. The most relevant in this work are the rod burst, hold-up by oxide shell, and eutectic reactions.

The rod burst and radionuclide release to the gap is assumed to occur at 900°C (1173K) for both Zr and FeCrAl, which accounts for the lack of experimental data from FeCrAl rod burst experiments and is consistent with previous work [60] [66].

The hold-up by oxide shell model aims to capture the mechanical effect of the outer shell formed around the Zr cladding when oxidation occurs with steam. This oxide shell has a higher melting temperature than the underlying cladding and has been observed to maintain structural integrity even as the unoxidized cladding material inside the shell melts away [67]. MELCOR allows a ZrO_2 shell to remain intact and able to support a melt up to 2400 K, after which a time-at-temperature failure mode was activated, and the cladding begins to fail. If the temperature reaches 2800 K, instant failure and collapse of the oxide shell is assumed. However, as this effect is not expected to be observed in FrCrAl cladding [60][68], the failure temperature for both shell hold-up and collapse is modeled as the oxide melting temperature for FeCrAl. This data is displayed in Table 3-6.

Table 3-6. MELCOR cladding failure temperature for Zr and FeCrAl.

Material	Rod Burst Onset (K)	Melting		Oxide Forced Failure	
		Metal (K)	Oxide (K)	Shell Melt Hold-up (K)	Collapse (K)
Zr	1173	2098	2990	2400	2800
FeCrAl	1173	1173	1901	1901	1901

Due to the ongoing development of the recent UDM model, there is currently no option to use the eutectics model with the FeCrAl cladding. However, preliminary experiments show that FeCrAl does not appear to form a eutectic with UO_2 [70][71]. Furthermore, previous work using older versions of MELCOR at ORNL advise against using the eutectic model for either Zr or FeCrAl [60]. Although the eutectics model was updated in MELCOR 2.2 and is now understood to be a promising modeling option, in this work the default model did not use the eutectics model for Zr or FeCrAl. Sensitivity analysis may instead be performed on the inclusion of the eutectics model for the Zr cladding model in future work.

3.2.6 Decay Heat and Radionuclides

MELCOR calculates the decay heat and radionuclide inventory of the model via two dedicated packages which consider fission products grouped into "classes," as described in Table 3-7.

Table 3-7. MELCOR decay heat and radionuclide classes.

Chemical Group	Header Element	Elements
Noble gases	XE	Xe, Kr, Rn, He, Ne, Ar, H, N
Alkali metals	CS	Cs, Rb, Li, Na, K, Fr, Cu
Alkaline earths	BA	Ba, Sr, Be, Mg, Ca, Ra, Es, Fm
Halogens	I2	I, Br, F, Cl, At
Chalcogens	TE	Te, Se, S, O, Po
Platinoids	RU	Ru, Pd, Rh, Ni, Re, Os, Ir, Pt, Au
Transition metals	MO	Mo, Tc, Nb, Fe, Cr, Mn, V, Co, Ta, W
Tetravalents	CE	Ce, Zr, Th, Np, Ti, Hf, Pa, Pu, C
Trivalents	LA	La, Pm, Sm, Y, Pr, Nd, Al, Sc, Ac, Eu, Gd, Tb, Dy, Ho, Er, Tm, Yb, Lu, Am, Cm, Bk, Cf
Uranium	UO2	U
More volatile main group metals	CD	Cd, Hg, Pb, Zn, As, Sb, Tl, Bi
Less volatile main group metals	AG	Sn, Ag, In, Ga, Ge
Boron	BO2	B, Si, P
Water	H_2O	'WT'
Concrete	CON	'CC'

Chemical Group	Header Element	Elements
Cesium iodide	CSI	-
Cesium molybdate	CSM	-

The decay heat package is responsible for defining the time-dependent decay heat, whether this is given as exact tabulated data or as an ANS or ORIGEN standard. This package also allows redefinition of the decay heat classes if desired by the user. The initial radionuclide mass inventories are usually defined in the decay heat package but may also be input in the radionuclide package, which also describes their distribution within the core and calculates their release and transport behavior.

The decay heat and radionuclide inventory definition methods for this model are the topic of ongoing discussion due to the complexities involved in the use of HBU fuel. Ultimately, it would be desirable to use the detailed time-dependent isotopic decay heat data and fission product masses from the VERA model of the Zion reactor. One limitation of this method is that isotope-specific decay heat data is not available from VERA. This can in principle be derived offline but this is time-consuming and may have limited benefit. A simplified approach using the ANS standard decay heat curves and an applied scaling factor in MELCOR is also considered, which is anticipated to capture key phenomena. The different methods are listed below with a description of the decay heat package dataflow.

MELCOR then uses this decay heat to calculate the initial radionuclide inventories using data from previously performed ORIGEN simulations. Two sets of ORIGEN data are available, from PWR or BWR calculations, and the user-specified reactor operating power and time define how to generate initial inventories from this default reactor-specific data. The spatial distribution of fission products, both in the whole core and the fuel-cladding gap, is defined using a fractional description of total fission products in the radionuclide package. The spatial power distribution is also defined in the radionuclide package. At present this data has not been updated from the original 15 × 15 Zion model. However, once the detailed VERA reactor power distribution becomes available this will be included in MELCOR.

The decay heat calculation using the ANS standard method takes the user-specified operating time with a constant reactor power, assumes energy release per fission is independent of time, and finds the full-core decay heat power, $P_{core}(t)$, by:

$$P_{core}(t) = M_{user} G(t) \sum_{i=1}^{3} \frac{P_i F_i(t,T)}{Q_i} + P_{dHe}(t,T) \quad (7)$$

where:

M_{user} = user-input multiplier (default = 1)

$G(t)$ = neutron capture correction factor

t = time since reactor shutdown (s)

i = nuclide index

T = reactor operating time (s)

P_i = power from fission of nuclide i (W)

$F_i(t,T)$ = decay power due to nuclide i (MeV/fission)

Q_i = energy per fission of nuclide i (MeV/fission).

This amounts to a sum over the operating time of contributions from the fissions of key nuclides. The decay power from a fission reduces exponentially with time. Therefore, the contribution from a fission that occurred >1 year ago appears negligible. As a result, the direct effect of longer operation time on

decay heat is likely to be small. A secondary effect occurs due to a change in the ratio of U-235, Pu-239, and U-238 fissions. This can be specified in MELCOR but requires data on the relative fission rates at higher burnups. This can in principle be taken from VERA. Here, this effect is neglected as it is assumed to be second order.

3.2.7 LBLOCA Scenario

The accident scenario used for the MELCOR Zion model was defined in the original NRC model [41]. The model was revised for the source term analysis as a consequence of LBLOCA. A double-ended guillotine break occurred with an initial failure of the LPSI system due to unverifiable equipment failure. This model assumed that LPSI capability restored at 27 minutes (1620 seconds) after the initiation of the LOCA event. The core will be partly damaged when core is uncovered by coolant and melted until core is reflooded again. It is noted that input detail is not publicly available. Figure 3-2 shows nodailization scheme for MELCOR modeling.

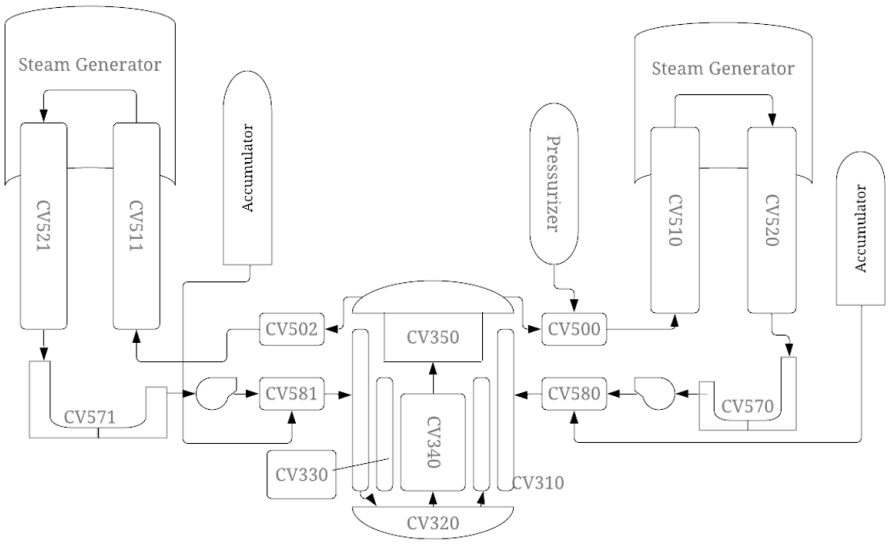

Figure 3-2. Nodalization for MELCOR modeling

MELCOR control functions are used to dynamically change parameters depending on the accident progression. This allows system responses to be defined for changing reactor conditions and automatically trigger during the simulation. Most of the control functions were defined in this way and depend on the values of specific variables, but a select number are constructed to trigger at particular times in the simulation as user-defined events. These are listed in Table 3-8. The timings of these user-defined events are the same for both the Zr and FeCrAl models.

Table 3-8. User-defined events in LBLOCA scenario.

Event	Time (s)
Simulation starts	−200
Double-ended rupture in pressurizer loop	0
Reactor SCRAM	0
LPSI reactivation	1620
Simulation end	21600

3.3 MELCOR Simulation Results

3.3.1 Comparison with Reference MELCOR Results: Zr-clad fuel

The results MELCOR 2.2 with Zr-clad fuel model are compared with the SNL/NRC results for MELCOR 1.8.5 and 2.0 in Figure 3-3 to Figure 3-7. The unaltered MELCOR input (with 15 × 15 fuel) was first run to quantify differences between versions of MELCOR. Some differences are to be anticipated due to the continued evolution of the code and the sensitivity of outcomes in beyond-design basis accidents to relatively small variations in conditions and assumptions. Next, the case with 17 × 17 fuel is compared to the case with 15 × 15 fuel.

The core water level of all models dropped below the top of the active fuel, with the 2.2 results showing a drop of roughly 3 m in a behavior that is more similar to the drop and recovery of the 1.8.5 water level results than the 2.0. The water level in the 2.2 results notably does not recover fully to stay above the level of the active fuel. The containment pressure for the 2.2 model matches well with the 2.0 results, including the rise when the containment sprays switch from injection mode to recirculation mode.

The fuel temperature shows different behavior in the 2.2 results, with fuel melting not penetrating as far down as seen for the 2.0 model. In the 2.0 results, fuel melting reaches axial levels L8 and L9, whereas the 2.2 results do not observe fuel melting until L11 for the 15 × 15 model and L12 for the 17 × 17 model.[3] It is unknown from the previous results which axial level the 1.8.5 model fuel melt reaches. The higher fuel melt seen for 17 × 17 fuel may merit further investigation, but it is noted that the clad temperatures are very similar to the 15 × 15 model, indicating sensitivity to small changes in initial conditions (a feature of severe accident analysis, and hence the increased fuel melt could perhaps be due to thinner clad).

The hydrogen production results for 2.2 match well with the previous MELCOR results, which observed a range of around 240–275 kg between 1.8.5 and 2.0. Less hydrogen is produced for the 15 × 15 model than for the 17 × 17 model, which could be since the fuel in the 17 × 17 model is uncovered for longer as shown in Figure 3-3 and/or larger pin surface area.

The total radioactive mass released from the core in the 2.2 model is comparable with the 1.8.5 results but significantly lower than the 2.0 results. This may be due to a known model error in 2.0 in the radionuclide package, where the mass release reported for some classes sometimes exceeded the total mass available for the class as noted in the change log [49]. This error was fixed in Version 2.2, which may explain the discrepancy. The higher radioactive mass release for the 17 × 17 model is consistent with increased fuel melt.

[3] See Figure 3-1 for level labels.

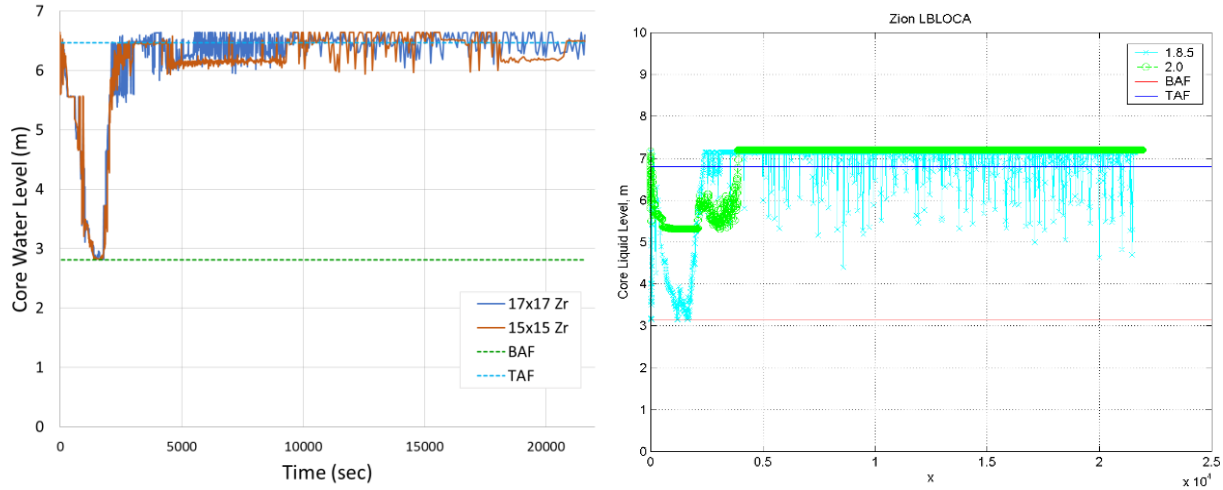

Figure 3-3. Core water level (left: MELCOR 2.2, right: MELCORE 1.8.5 and 2.0 [48]).[4]

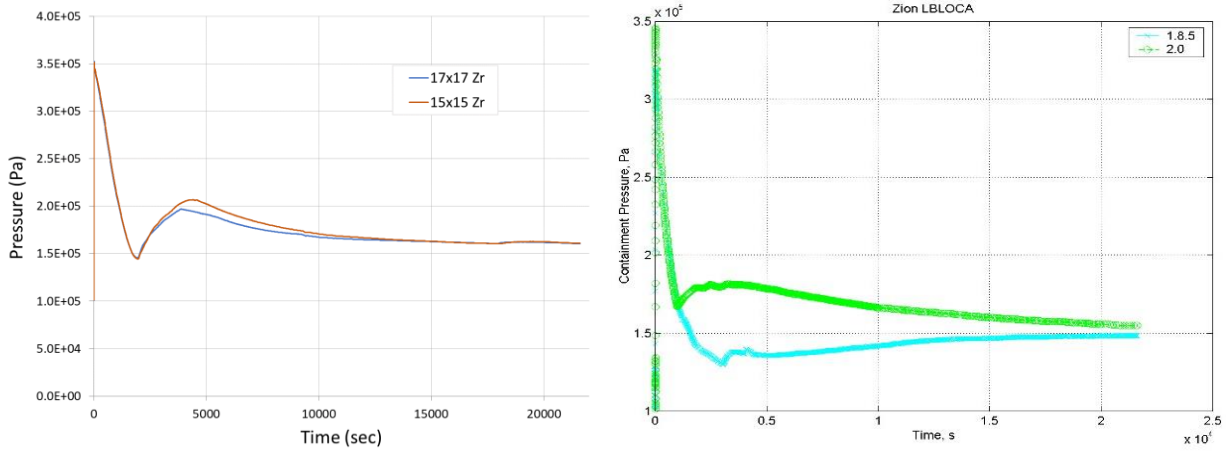

Figure 3-4. Containment pressure (left: MELCOR 2.2, right: MELCORE 1.8.5 and 2.0 [48]).

[4] BAF: Bottom Active Fuel, TAF: Top Active Fuel.

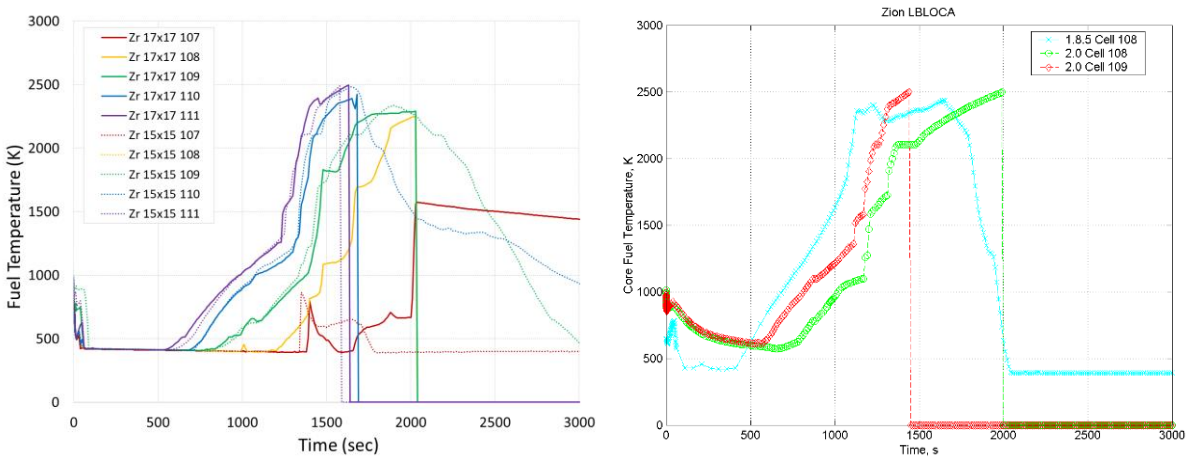

Figure 3-5. Fuel temperature (left: MELCOR 2.2, right: MELCORE 1.8.5 and 2.0 [48]).

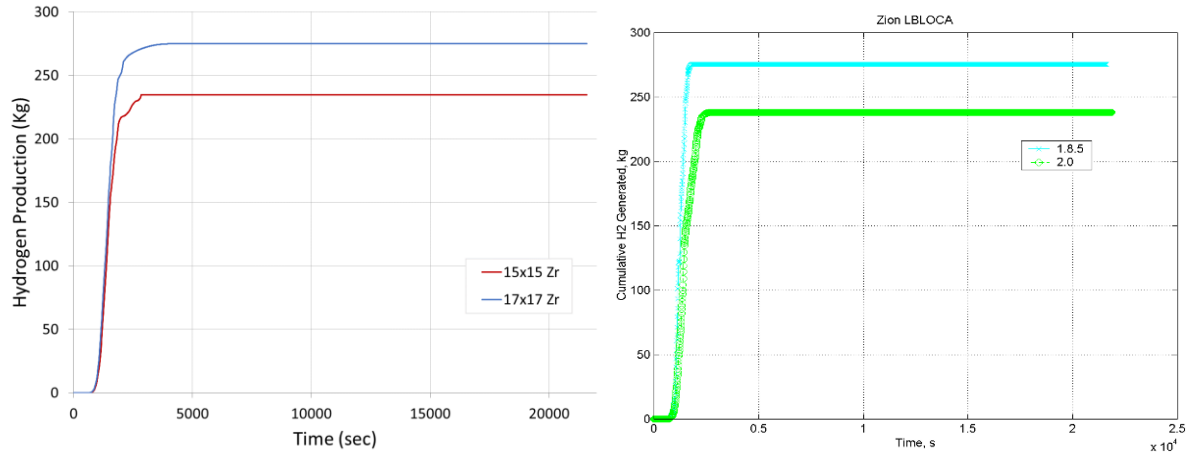

Figure 3-6. Hydrogen production (left: MELCOR 2.2, right: MELCORE 1.8.5 and 2.0 [48]).

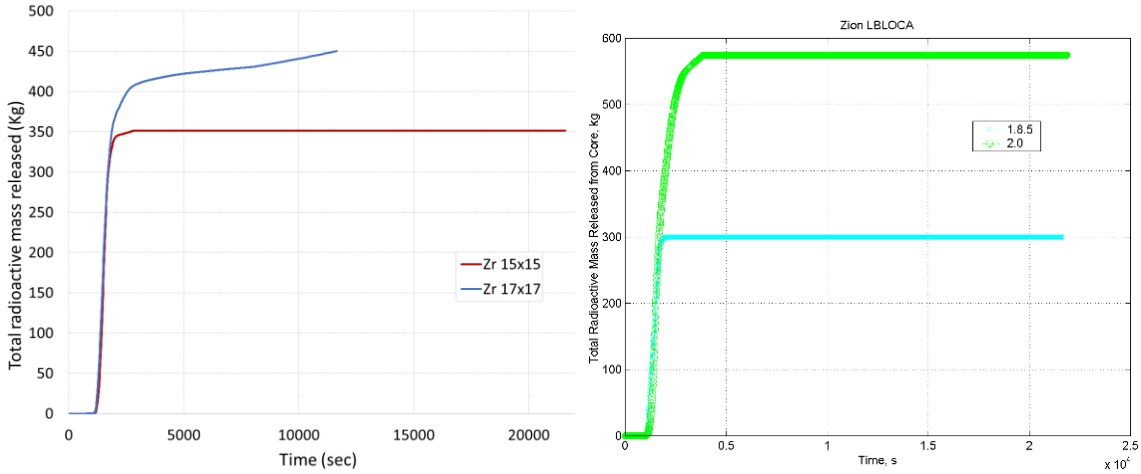

Figure 3-7. Total radioactive mass release from the core (left: MELCOR 2.2, right: MELCORE 1.8.5 and 2.0 [48]).

3.3.2 FeCrAl and Zr-clad Fuel Core Comparison: 18 months case

The MELCOR 2.2 results of FeCrAl-clad fuel core model was compared with baseline Zr-clad fuel core model. Figure 3-8 shows the core water level with Zr and FeCrAl cladding. The results of both Zr-clad fuel and FeCrAl-clad fuel were similar. Water level rises once the LPSI is restarted at 1620 seconds.

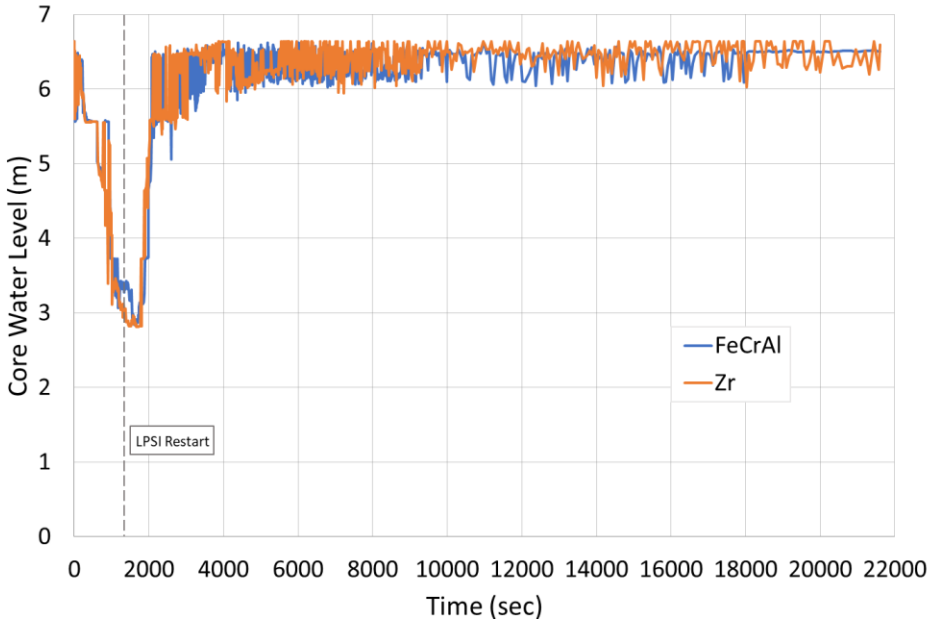

Figure 3-8. Core water level comparison between Zr and FeCrAl-clad fuel.

The clad temperature in the radial center of the core was compared between Zr and FeCrAl at different axial levels, as shown in Figure 3-9. Zr has a higher melting temperature than FeCrAl (i.e., Zr melts at 2128K and FeCrAl melts at 1773K). However, the FeCrAl cladding heats up more slowly, understood to be due to superior oxidation performance. As a result, the melting extends further down the core with Zr-clad fuel compared to FeCrAl. The melt extends to the L8 axial node (second in the core) for Zr-clad fuel, and only the L11 (fifth in the core) for FeCrAl. Considering the accident scenario, Zr-clad fuel starts candling at 990 seconds and starts fuel collapse near 1020 seconds than ends near 2000 seconds. However, FeCrAl-clad fuel starts candling around 1150 seconds, collapse begins near 1510 seconds and ends near 1940 seconds. In other words, the FeCrAl-clad fuel failure starts 200 to ~500 seconds later at same conditions of the accident which gains buffer until LPSI restarts. The Zr-clad fuel already started collapsing about 600 seconds earlier than LPSI restarts while FeCrAl-clad fuel started collapsing just 100 seconds before LPSI injection.

It is noted that the fuel failure mechanism needs to be further studied by sensitivity studies on LPSI reactivation time and fuel oxidation model which may need verification for FeCrAl material.

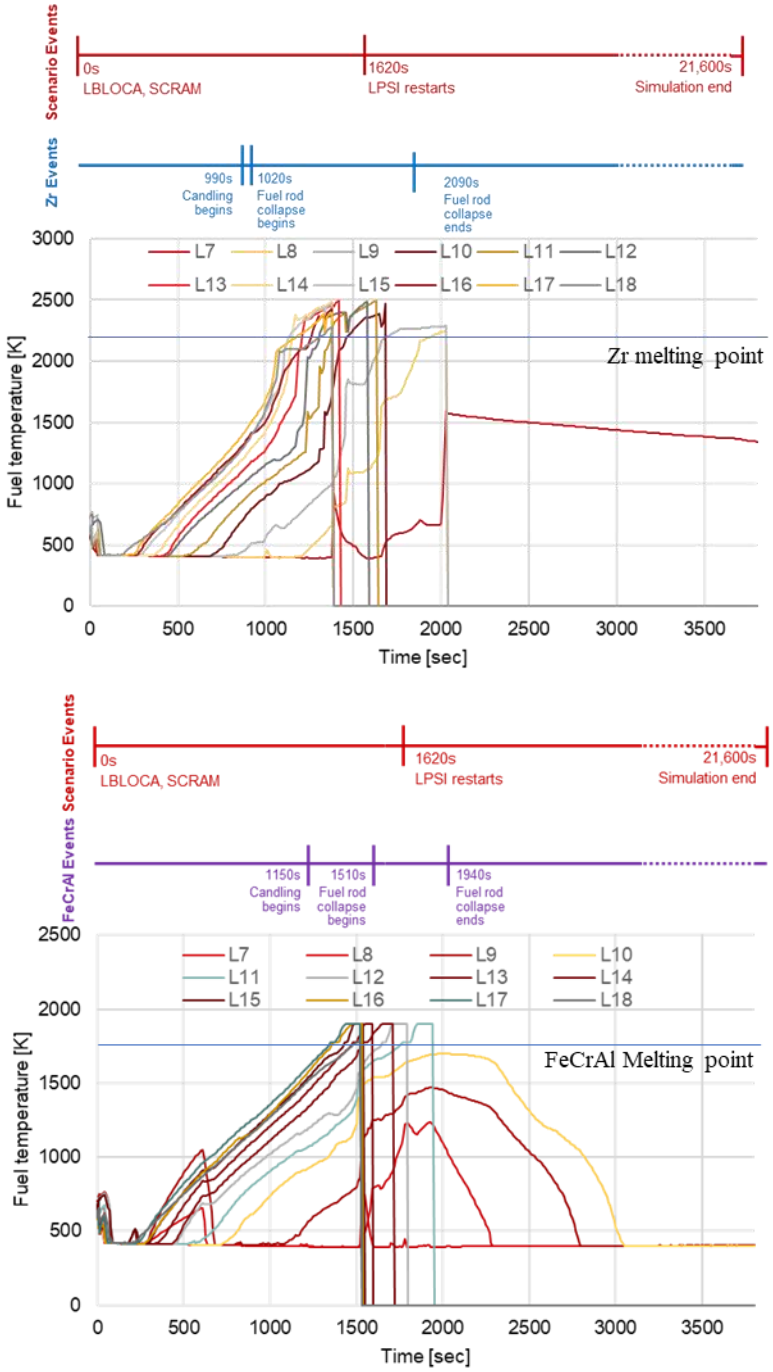

Figure 3-9. Axial fuel temperature (top: Zr-clad fuel, bottom: FeCrAl-clad fuel).

The hydrogen generation rate is shown in Figure 3-10. The hydrogen generation rate is appreciably lower for FeCrAl, but this is not dramatic. The delayed hydrogen production is due to the higher activation temperature and energy at temperatures up to 1773 K. However, beyond this, the oxidation rate is extremely high, as shown in Table 3-5. The modeling of this effect varies in the literature but has previously been modeled for example in the reference [10].

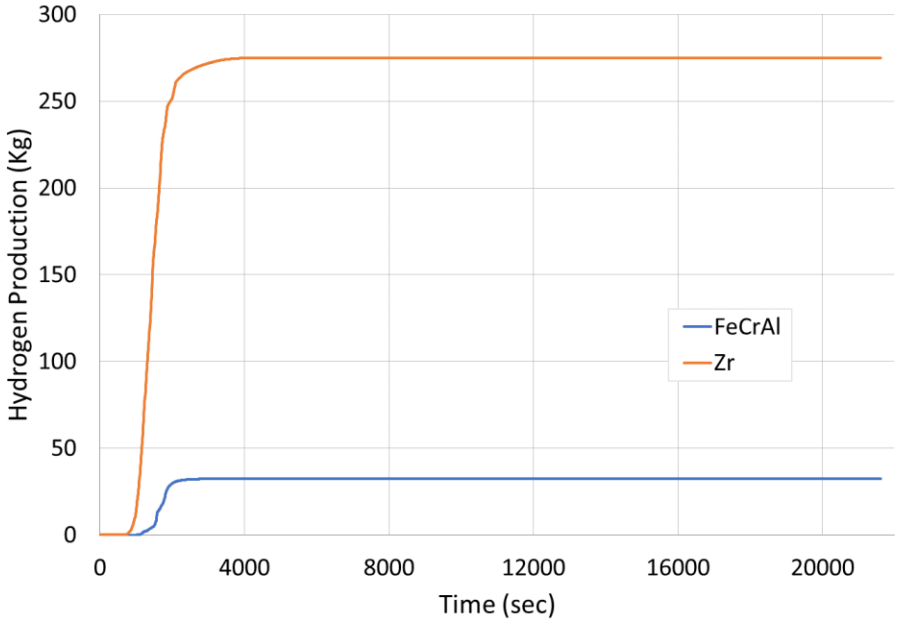

Figure 3-10. Hydrogen production between Zr and FeCrAl-clad fuel.

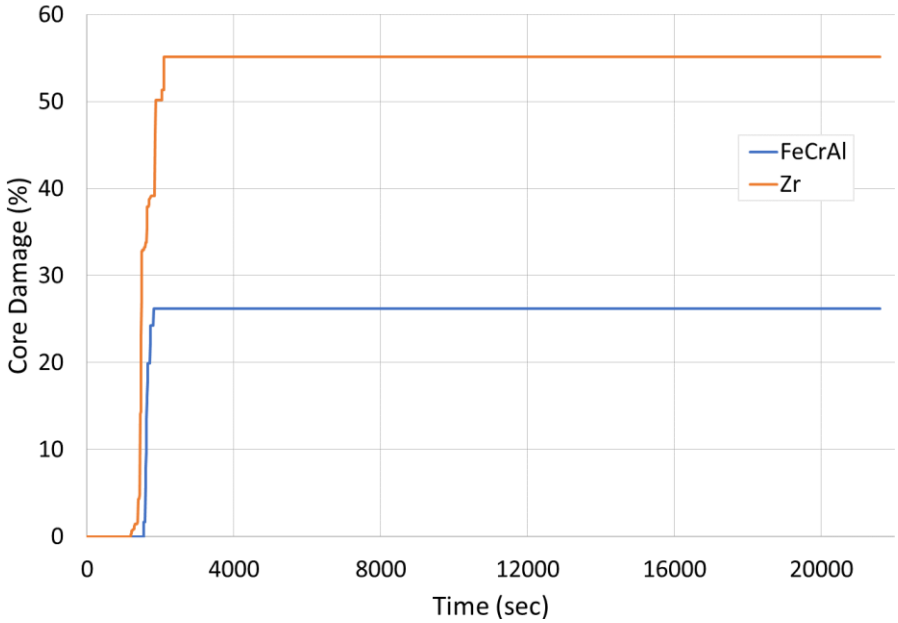

Figure 3-11. Core damage rate comparison between Zr and FeCrAl-clad fuel.

Figure 3-12 to Figure 3-13 shows amount of released fission products from Zr and FeCrAl-clad fuels. The figures show total, major fission product elements defined in MELCOR and comparison. The amount is significantly lower in FeCrAl than for Zr-clad fuel, driven by the lower fuel melt. This reduction in fission product release, albeit for specific accident scenarios such as this, may contribute incrementally to a reduced source term and hence demonstrate available safety margin for higher burnup operation.

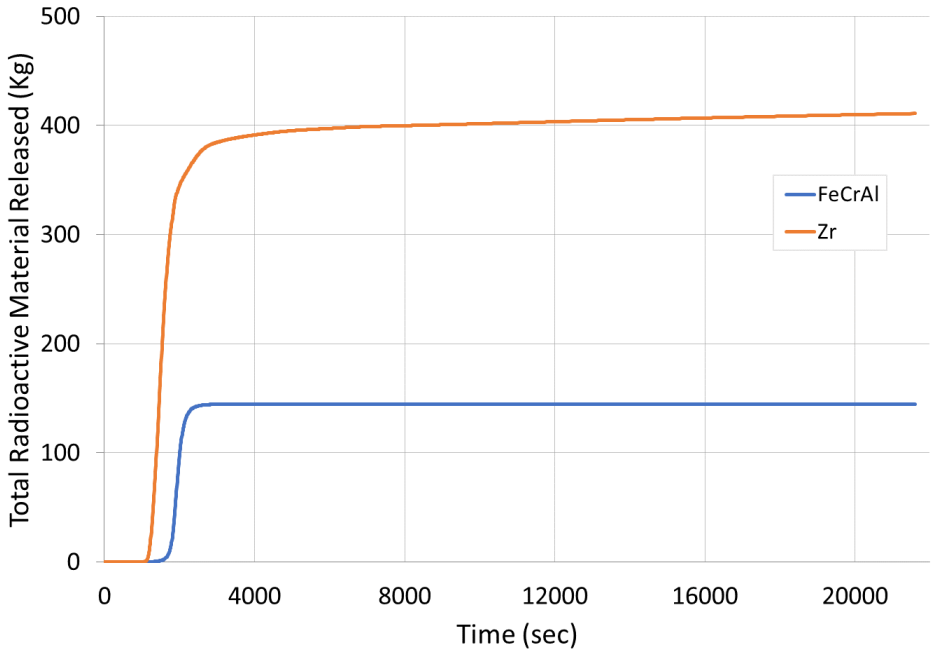

Figure 3-12. Total fission product release comparison between Zr and FeCrAl-clad fuel.

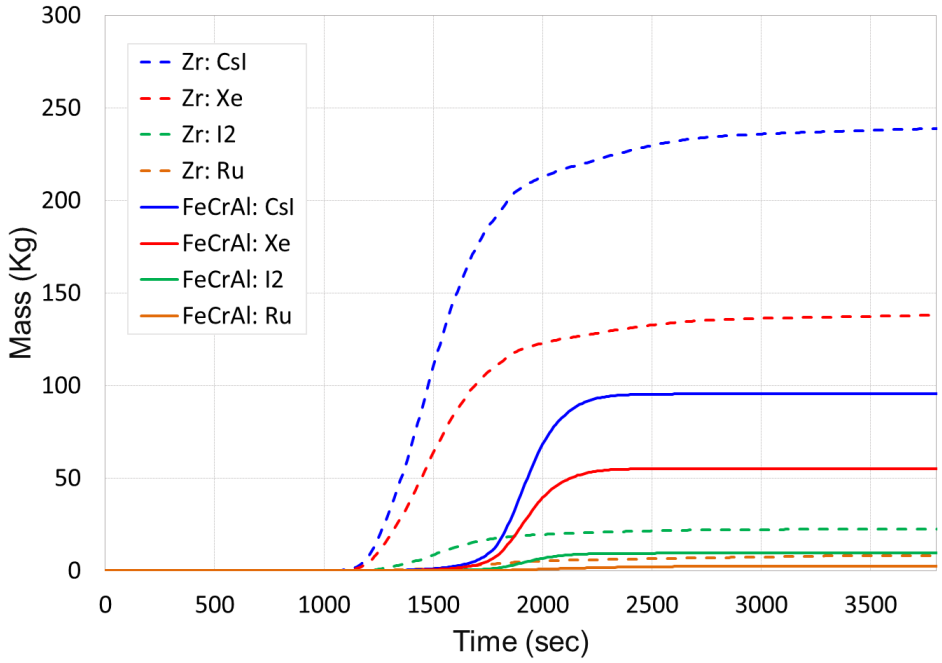

Figure 3-13. Comparison of the major released major radioactive materials between Zr (dashed lines) and FeCrAl (solid lines) clad fuels.

Figure 3-14 shows core melting result at the end of the simulation (21600 seconds). Before meltdown all fuel rods are intact as shown with purple color rod. Before meltdown fuel rods (purple color) in the coolant (blue) are intact. On the right side of the figure shows molten fuel (green), and void from core melt (dark green) and void due to coolant boiling (white). At the end of simulation, melted fuels in green and brown are stacked at the center of the core and bottom of the reactor vessel as a form of corium. The

vacant or steam are shown in white bubbles. It is clear that fuel damage and steam amount are less in FeCrAl-clad fuel core.

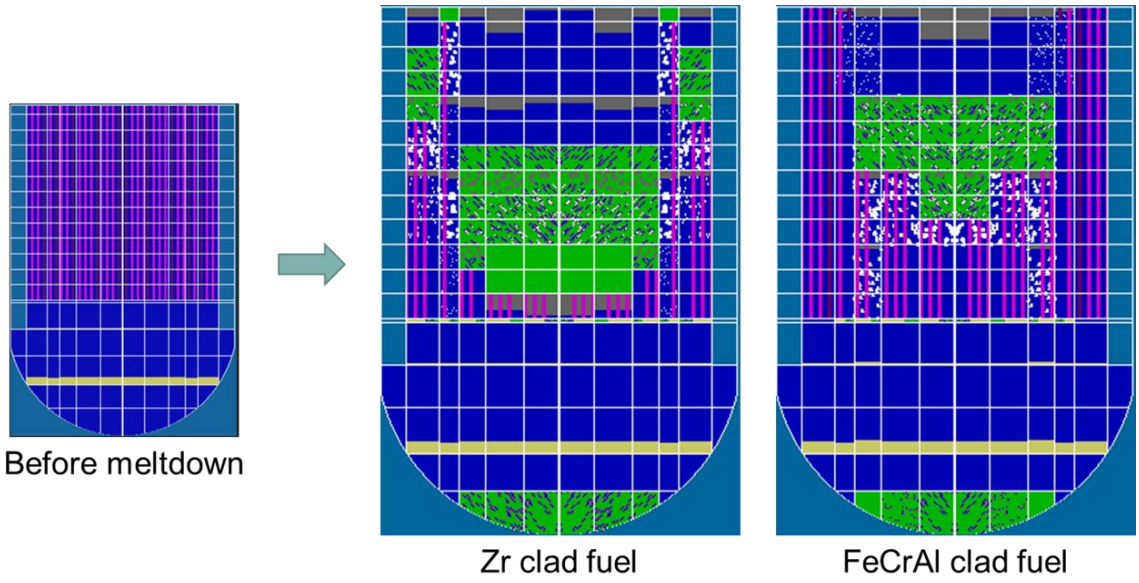

Figure 3-14. Core meltdown result at completion of simulation (21600 seconds).

3.3.3 24 Months Operation Cycle with FeCrAl-clad Fuel Core

As described in Section 3.2.6, the decay heat and fission product inventory models for HBU fuel are not yet available due to complexity of HBU fuel characteristics and isotope-specific decay heat data is not available from VERA simulation. The most applicable method is using scaling from 18-month cycle standard ANS decay heat curves to 24-monthe. The amount of decay heat was assumed to be proportionally from the end of equilibrium cycle (EOEC) burnup of 18-month cycle. For the source term analysis of the 24-month cycle, the SCALE code was first applied based on the estimated decay heat power from 24-month cycle then applied to MELCOR source term analysis. The SCALE code has advantage of producing inventories of each fission product by using averaged burnup and fuel enrichment data calculated from VERA code. The research will continue to develop appropriate HBU decay heat and fission product inventory models.

Figure 3-15, Figure 3-16 and Figure 3-17 shows comparison between 18- and 24-month cycle results of produced hydrogen, core damage rate and total fission product generated, respectively. The values from 24-month cycle shows slightly higher than those of 18-month cycle.

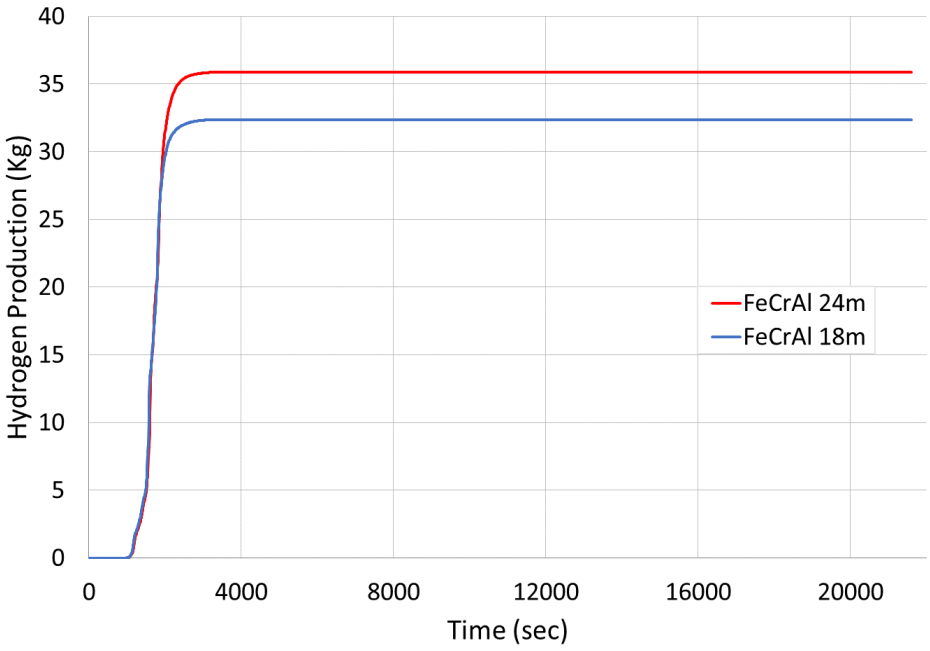

Figure 3-15. Hydrogen production between 18- and 24-month cycle of FeCrAl-clad fuel.

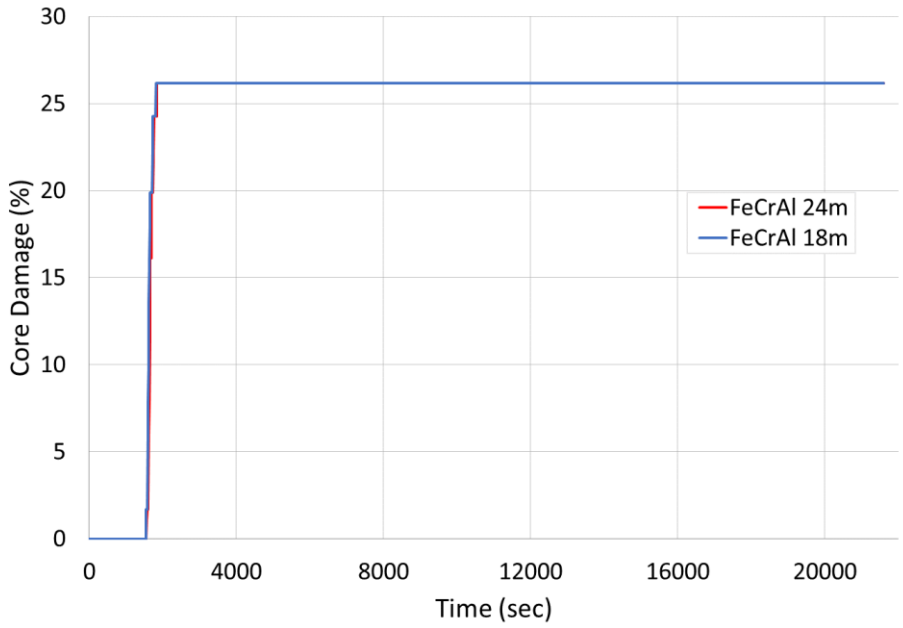

Figure 3-16. Core damage rate comparison between 18- and 24-month cycle of FeCrAl-clad fuel.

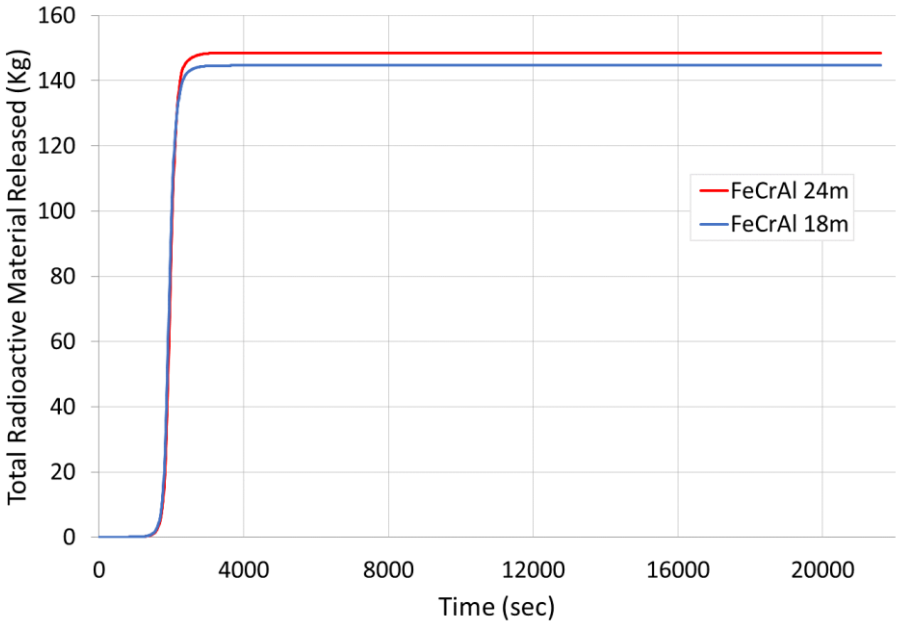

Figure 3-17. Total fission product release comparison between 18- and 24-month cycle of FeCrAl-clad fuel.

4. CONCLUSIONS AND FUTURE WORK

This study was focused on the radioactive source term analysis during the severe accident of the FeCrAl ATF loaded Westinghouse Type 4-loop PWR. Based on the WBN-1 NPP reactor core, a 17 × 17 FeCrAl-clad fuel loaded core with 24-month operation cycle was developed. First, Zr-clad fuel with conventional 18-month cycle core was developed compared with reference data then applied to FeCrAl-clad fuel. Neutron penalty due to higher absorption cross section of FeCrAl cladding was studied and optimal enrichment was proposed. For 24-month operation cycle the actual EFPD was found 697.4. The enrichment of the fuel was increase higher than 7 wt.% to compensate neutron penalty from FeCrAl cladding. The peak pin burnup was reached to 81.87 GWD/MTU. It is noted that increasing the enrichment also need increase of burnable poison to avoid undesired reactivity and thermal feedback effects.

Developed FeCrAl-clad fuel loaded 18- and 24-month operation cycle reactor core data were sent to simulate severe accident by using MELCOR 2.2 by using Zion NPP model. The reactor model has been verified with previous versions of MELCOR and compared with references. The thermophysical properties of FeCrAl cladding were applied by user-defined material feature of the code. The guillotine break LBLOCA was simulated with the assumption of the ECCS was initially failed and recovered by the operator at 27 minutes from the reactor transient. Both FeCrAl cladding failure model and decay heat model were applied. For the 24-month cycle, the decay heat and fission product inventories were scaled up from 18-month cycle. This enables the core water level to be recovered and limits fission product release.

Under such a scenario, the results indicate that the previously established delay in fuel failure with FeCrAl fuel is somewhat beneficial in limiting overall fission product release; therefore, this contributes to a reduction in the source term. Generated hydrogen and source term are compared with Zr-clad fuel and found FeCrAl-clad fuel can significantly reduce the major source term, up to three times less. Slower fuel failure mechanism behavior of ATF is known due to the smaller oxidation rate compared to Zr-clad fuel may reduce cladding embrittlement. However, due to lack of experimental data for ATF and HBU fuel cycle, there might be uncertainties in simulation. Hence, further study is necessary.

A 24-month high burnup core with FeCrAl-clad is further estimated to have reduced fission product release compared to the 18-month cycle. Produced hydrogen and source term and core damage rate were slightly higher in 24-month. The work will continue to upgrade the decay heat and fission product inventory model for HBU fuel cycle.

Following issues and needs were identified:

- The geometry of the FeCrAl and Zr-clad fuels were identical. Thinner FeCrAl cladding has been considered to reduce the neutron penalty and these other types of FeCrAl-clad fuel need to be addressed.
- The FeCrAl-clad fuel core design needs to apply different burnable poison options, such as gadolinium rods, to improve core performance.
- The ATF (not only FeCrAl) core design and equilibrium cycle development needs fuel performance and thermal-hydraulic analysis feedback including DBA analysis. Current core design uses safety constraints (i.e., power peaking factors) from Zr-clad fuel core design due to lack of transient test data of FeCrAl-clad fuel.
- Need of the explicit simulation of the accident scenario with the higher burnup fuel definition from VERA-CS. This is anticipated to include (1) axial and radial power distribution for high burnup core, (2) explicit radionuclide inventory from the core model, and (3) best estimate decay heat from the core model.

- Need of the sensitivity analysis with different LPSI injection times to gain further insight into the sensitivity to this parameter. In general, it is important to perform sensitivity analysis with MELCOR as the progression of severe accidents is highly sensitive to models and initial conditions and bifurcation behavior can be observed. This is already apparent from this report, where relatively small changes (e.g., 15×15 compared to 17×17 fuel) can lead to appreciably different outcomes.
- Plant specific LOCA scenarios and other DBA analysis are needed to understand system feedback during the accident.
- Since ATF technology is still under development, the experimental data is significantly missing. This leads less credential on M&S results. Comprehensive code-to-code and code-to-experiment benchmarks are necessary for licensing application.
- Fuel failure mechanisms for ATF and HBU fuel cycle need to be clarified. It is known that higher irradiation and higher oxidation rate accelerates cladding embrittlement in Zr-clad fuel. However, it is still uncertain for the fuel failure mechanisms of ATF and HBU fuel cycle. Related experiment is planned by INL [4].

Future works will include:

- Assessment of technical gaps and needs for safety analysis in FFRD under various DBA of P/BWR loaded with increased enrichment ATF and extended burnup. This includes review on available accident analysis computational tools and experiments for code update and verification and validation. This activity supports ongoing activity with industry and will support immediate need for ATF licensing purpose.
- Safety analysis of limiting anticipated operational occurrences (AOO) and DBAs of ATF loaded 4-loop typical PWR with higher enrichment and burnup by using RELAP5-3D. Existing fuel failure model (e.g., FFRD) in RELAP5-3D will be verified and updated as needed. The fuel failure result will be used for initial thermal-hydraulic conditions for the source term dose calculation by MELCOR/MACCS.
- Environmental impact analysis from the leakage of major radioisotopes released due to severe accident of higher enriched FeCrAl cladding ATF loaded PWR with high burnup fuel cycle by using MELCOR/MACCS accident consequence analysis codes. The analysis will consider variety of physical phenomena, including building wake and plume.

5. REFERENCES

[1] Stewart, R., C. Blakely, H. Zhang. (2021) "Investigation of a two-year cycle pressurized water reactor core design with increased enrichment and extended burnup limits." *Nuclear Engineering and Design,* 376.

[2] U.S. NRC. (2021) "Interpretation of Research on Fuel Fragmentation, Relocation, and Dispersal at High Burnup." RIL 2021-13.

[3] U.S. NRC. (2022) "Regulatory Framework Applicability Assessment and Licensing Pathway Diagram for the Licensing of ATF-Concept, Higher Burnup, and Increased Enrichment Fuels".

[4] Kamerman, D., Jensen, C., Wachs, D., Woolstenhulme., N., (2020) "High-burnup Experiments in Reactivity Initiated Accidents (HERA)", INL/EXT-20-57844, Idaho National Laboratory.

[5] Shirvan, K. (2020) "Implications of accident tolerant fuels on thermal-hydraulic research." *Nuclear Engineering and Design* 358: 110432.

[6] Rebak, R. B., K. A. Terrani, W. P. Gassmann, J. B. Williams, and K. L. Ledford. (2017) "Improving Nuclear Power Plant Safety with FeCrAl Alloy Fuel Cladding." *MRSAdvances* 2. no. 21–22: 1217–1224.

[7] Parisi, C., Z. Ma, D. Mandelli, N. A. Anderson, and H. Zhang. (2020) "Risk-Informed Safety Analysis for Accident Tolerant Fuels," Tech. Rep. INL/CON-19-53223-Rev.000, Idaho National Laboratory.

[8] Jin, Y. and K. Shirvan. (2021) "Assessment of coated cladding impact on large-break LOCA with TRACE-DAKOTA." *Nuclear Engineering and Design* 374: 111036.

[9] Guo, R. Dailey, T. Feng, Y. Zhou, Z. Sun, M. L. Corradini, and J. Wang. (2021) "Uncertainty analysis of ATF Cr-coated-Zircaloy on BWR in-vessel accident progression during a station blackout." *Reliability Engineering & System Safety* 213: 107770.

[10] Wang, J., R. Dailey, Z. Guo, Y. Zhou, P. Humrickhouse, and M. L. Corradini. (2021) "Accident tolerant fuels (FeCrAl Cladding & Coating) performance analysis in Boiling Water Reactor (BWR) by the MELCOR 1.8.6 UDGC." *Nuclear Engineering and Design* 371: 110974.

[11] Gurgen, A., and K. Shirvan. (2018) "Estimation of coping time in pressurized water reactors for near term accident tolerant fuel claddings." *Nuclear Engineering and Design* 337: 38–50.

[12] Rearden, Bradley T., Jessee M. A. (2018), "SCALE code system", No. ORNL/TM-2005/39 Version 6.2.3, Oak Ridge National Lab (ORNL), Oak Ridge, TN 2018

[13] Quist, A. (2011) "VERA version 1.3 user manual and documentation." LA-UR-11-00101, Los Alamos National Laboratory.

[14] Sandia National Laboratory. (2022) "MELCOR." Sandia National Laboratory. https://energy.sandia.gov/programs/nuclear-energy/nuclear-energy-safety-security/melcor/

[15] Sandia National Laboratoy, (2022) "MACCS." Sandia National Laboratory. https://maccs.sandia.gov/maccs.aspx.

[16] U.S. NRC. (1996) "10CFR Part 100: Reactor Site Criteria".

[17] U.S. NRC. (1995) "Accident Source Terms for Light-Water Nuclear Power Plants", NUREG-1465.

[18] U.S. NRC. (1990) "Severe Accident Risks: An Assessment for Five U.S. Nuclear Power Plants", NUREG-1150.

[19] Ashbaugh, S. et al., (2010) "Accident Source Terms for Pressurized Water Reactors with High-Burnup Cores Calculated Using MELCOR 1.8.5." SAND2008-6664, Sandia National Laboratory.

[20] Powers, D. et al. (2011) "Accident Source Terms for Light-Water Nuclear Power Plants Using High-Burnup or MOX Fuel." SAND2011-0128, Sandia National Laboratory.

[21] U.S. NRC. (2022) "Alternative Radiological Source Terms for Evaluating Design Basis Accidents at Nuclear Power Reactors", DG-1389

[22] Ott, L.J., Robb, K.R., Wang, D, (2014) "Preliminary assessment of accident-tolerant fuels on LWR performance during normal operation and under DB and BDB accident conditions", *Journal of Nuclear Materials* 448: 520-533.

[23] Allen, T., R. Konings, A. Motta. (2012) "Corrosion of zirconium alloys." *Comprehensive Nuclear Materials* 5: 49-68.

[24] Terrani, K., S. Zinkle, L. Snead. (2017) "Advanced oxidation-resistant iron-based alloys for LWR fuel cladding." *Journal of Nuclear Materials* 448. no. 1-3: 420-435.

[25] Tang, C., M. Stueber, H. Seifert, M. Steinbrueck. (2017) "Protective coatings on zirconium-based alloys as accident-tolerant fuel (ATF) claddings." *Corrosion reviews* 35, no. 3: 141–165.

[26] Pellegrini, M., et al. (2016) "Benchmark study of the accident at the Fukushima Daiichi NPS: best-estimate case comparison." *Nuclear Technology* 196, no. 2: 198–210.

[27] Sehgal, B. (2006) "Light water reactor (LWR) safety." *Nuclear Engineering and Technology* 38, no. 8: 697–732.

[28] OECD, (2018) "State-of-the-art report on light water reactor accident-tolerant fuels." Nuclear Energy Agency.

[29] Kim, H., et al., (2013) "High-temperature oxidation behavior of Cr-coated zirconium alloy." Proceeding of LWR Fuel Performance Meeting/TopFuel, Charlotte, USA, 842: 846.

[30] Kim, H., et al., (2016) "Development status of accident-tolerant fuel for light water reactors in Korea." *Nuclear Engineering and Technology* 48, no. 1: 1-15.

[31] Rebak, R., et al., (2015) "Assessment of advanced steels as accident tolerant fuel cladding for commercial light water reactors." 17th International Conference on Environmental Degradation of Materials in Nuclear Power Systems – Water Reactors. August 9-13, 2015. Ottawa, Ontario, Canada.

[32] Field, K., K. M. Snead, Y. Yamamoto, K. Terrani (2018) "Handbook on the material properties of FeCrAl alloys for nuclear power production applications." ORNL/SPR-2018/905, Oak Ridge National Laboratory.

[33] George, N., K. Terrani, J. Powers, (2013) "Neutronic analysis of candidate accident-tolerant iron alloy cladding concepts." ORNL/TM-2013-121, Oak Ridge National Laboratory.

[34] Yamashita, S., F. Nagase, Y. Kaji, M. Kurata, (2016) "Establishment of technical basis to implement accident tolerant fuels and component to existing LWRs." American Nuclear Society Conference.

[35] Godfrey, A. (2014) "VERA core physics benchmark progression problem specifications." CASL-U-2012-0131-004, Revision 4.

[36] Stuart, S. (2013) "Nuclear Power Generation: Modern Power Station Practice." *Elsevier*.

[37] Zhang, H., et al. (2019) “Fuel rod burst potential evaluation under LOCA conditions for an existing plant with extended burnup exceeding the current limit by 20%. INL/EXT-19-55888, Idaho National Laboratory.

[38] Skutch, J., W. Slagle, Y. Sung. (1997) “TVA Watts Bar Unit 1 Cycle 2 Reload Safety Evaluation.” Tennessee Valley Authority, Westinghouse Electric Corporation.

[39] Kingsley, O., H. Khang, J. Yong, J. Hou. (2022) “Neutronics Assessment of Advanced Fuel Claddings in the Equilibrium LWR Core Design.” *Proceedings of ANS 2022 Winter meeting*. Under review.

[40] Pilch, M. M. (1998) “Evaluation of Radiological Consequences of Design Basis Accidents at Operating Reactors Using The Revised Source Term,” letter Report for Office of Nuclear Regulatory Research, U.S. Nuclear Regulatory Commission, Sandia National Laboratory.

[41] NRC. (2022) “Zion Units 1 & 2.” Nuclear Regulatory Commission. Nuclear Regulatory Commission. https://www.nrc.gov/info-finder/decommissioning/power-reactor/zionnuclear-power-station-units-1-2.html.

[42] Impink, J., and I. I. I. Guthrie. (1979) “Reactor core physics design and operating data for Cycles 1 and 2 of the Zion Unit 2 PWR power plant. Final report.” EPRI-NP-1232, Carnegie-Mellon Univ., Pittsburgh, PA (USA). Nuclear Science and Engineering Div.

[43] Soffer, L., S. Burson, C. Ferrell, R. Lee, and J. Ridgely. (1995) “Accident source terms for Light-Water Nuclear Power Plants Final Report.” Nuclear Regulatory Commission.

[44] Vierow, K. (2004) “Severe accident analysis of a PWR station blackout with the MELCOR, MAAP4 and SCDAP/RELAP5 codes.” *Nuclear Engineering and Design* 234: 129–145, Dec. 2004.

[45] Kmetyk, L., and L. Smith. (1994) “Summary of MELCOR 1.8.2 calculations for three LOCA sequences (AG, S2D, and S3D) at the Surry Plant.” NUREG/CR-6107; SAND-93-2042, Nuclear Regulatory Commission, Washington, DC (United States). Div. of Safety Issue Resolution; Sandia National Laboratory.

[46] Hidaka, A., K. Soda, and J. Sugimoto. (1995) “SCDAP/RELAP5 Analysis of Station Blackout with Pump Seal LOCA in Surry Plant.” *Journal of Nuclear Science and Technology* 32: 527–538.

[47] Gauntt, R. O., R. K. Cole, C. M. Erickson, R. G. Gido, R. D. Gasser, S. B. Rodriguez, M. F. Young, S. Ashbaugh, M. Leanard, and A. Hill. (2001) “MELCOR Computer Code Manuals Volume 3: Demonstration Problems Version 1.8.5.” NUREG/CR-6119; SAND2001-0929P; Vol. 3. Rev. 0. Sandia National Laboratory.

[48] Gauntt, R. O., R. K. Cole, C. M. Erickson, R. G. Gido, R. D. Gasser, S. B. Rodriguez, M. F. Young, S. Ashbaugh, M. Leanard, and A. Hill. (2000) “MELCOR Computer Code Manuals.” Nuclear Regulatory Commission.

[49] Humphries, L. L., J. L. Phillips, R. C. Schmidt, B. A. Beeny, D. L. Louie, and N. E. Bixler. (2020) “MELCOR Code Change History: Revision 14959 to 18019.” SAND2020-14302. Sandia National Laboratory.

[50] Houston, M. (1979) “Fuel performance annual report, period through December (1979) [PWR; BWR].” Nuclear Regulatory Commission. Office of Nuclear.

[51] Wang, J., M. Mccabe, T. Christopher Haskin, Y. Wu, G. Su, and M. L. Corradini. (2018) “Iron–Chromium–Aluminum (FeCrAl) Cladding Oxidation Kinetics and Auxiliary Feedwater Sensitivity Analysis—Short-Term Station Blackout Simulation of Surry Nuclear Power Plant.” *Journal of Nuclear Engineering and Radiation Science* 4.

[52] Wang, J., H. Yeom, P. Humrickhouse, K. Sridharan, and M. Corradini. (2020) “Effectiveness of Cr-Coated Zr-Alloy Clad in Delaying Fuel Degradation for a PWR During a Station Blackout Event,” *Nuclear Technology* 206: 467–477.

[53] Humphries, L. L., B. A. Beeny, F. Gelbard, D. L. Louie, J. L. Phillips, R. C. Schmidt, and N. E. Bixler. (2021) “MELCOR Computer Code Manuals Volume 1: Primer and Users’ Guide,” Tech. Rep. 2.2.19018. Sandia National Laboratory.

[54] Humphries, L. L., B. A. Beeny, F. Gelbard, T. Haskin, D. L. Louie, J. L. Phillips, R. C. Schmidt, and N. E. Bixler. (2021) “MELCOR Computer Code Manuals Volume 2: Reference Manual.” 2.2.18019. Sandia National Laboratory.

[55] Goodson, C., and K. Geelhood. (2020) “Degradation and Failure Phenomena of Accident Tolerant Fuel Concepts: FeCrAl Alloy Cladding,” PNNL-30445. Pacific Northwest National Laboratory.

[56] Robb, K. R. (2015) “Analysis of the FeCrAl Accident Tolerant Fuel Concept Benefits during BWR Station Blackout Accidents” Oak Ridge National Laboratory.

[57] Kanthal. (2021) “Kanthal APMT Construction Materials.” datasheet.

[58] Robb, K. R., J. W. McMurray, and K. A. Terrani. (2016) “Severe Accident Analysis of BWR Core Fueled with UO2/FeCrAl with Updated Materials and Melt Properties from Experiments,” ORNL/TM-2016/237. 68.

[59] Swiler, L., R. Schmidt, R. Williamson, and D. Perez. (2014) “Sensitivity Analysis of the Gap Heat Transfer Model in BISON.” SAND2014-18550. Sandia National Laboratory. 1160301. 540494.

[60] Robb, K. R., M. Howell, and L. J. Ott. (2017) “Parametric and Experimentally Informed BWR Severe Accident Analysis Using FeCrAl,” ORNL/SPR-2017/373, Oak Ridge National Laboratory.

[61] Pint, B. A., K. A. Terrani, Y. Yamamoto, and L. L. Snead. (2015) “Material Selection for Accident Tolerant Fuel Cladding.” *Metallurgical and Materials Transactions E* 2: 190–196.

[62] Ebrahimgol, H., M. Aghaie, and A. Zolfaghari. (2021) “Evaluation of ATFs in core degradation of a PWR in unmitigated SBLOCA,” *Annals of Nuclear Energy* 152: 107961.

[63] Urbanic, V. F., and T. R. Heidrick. (1978) “High-temperature oxidation of zircaloy-2 and zircaloy-4 in steam.” *Journal of Nuclear Materials* 75: 251–261.

[64] Pint, B. A., K. A. Terrani, M. P. Brady, T. Cheng, and J. R. Keiser. (2013) “High temperature oxidation of fuel cladding candidate materials in steam–hydrogen environments.” *Journal of Nuclear Materials* 440: 420–427.

[65] Brassfield, H., J. White, L. Sjodahl, and J. Bittel. (1968) “Recommended property and reaction kinetics data for use in evaluating a light-water-cooled reactor loss-of-coolant incident involving zircaloy-4-or 304-ss-clad UO_2.” General Electric Co., Cincinnati, OH (United States). Missile and Space Division.

[66] Massey, C. P., K. A. Terrani, S. N. Dryepondt, and B. A. Pint. (2016) “Cladding burst behavior of Fe-based alloys under LOCA.” *Journal of Nuclear Materials* 470: 128–138.

[67] Ghosh, S. (2019) “State-of-the-Art Reactor Consequence Analyses (SOARCA) Project Sequoyah Integrated Deterministic and Uncertainty Analyses.” Tech. Rep. NUREG/CR-7245, USNRC, Sandia National Laboratory.

[68] Pint, B. A., (2017) “Performance of FeCrAl for accident-tolerant fuel cladding in high-temperature steam.” *Corrosion Reviews* 35, no. 3: 167–175.

[69] Barrachin, M., D. Gavillet, R. Dubourg, and A. De Bremaecker. (2014) “Fuel and fission product behaviour in early phases of a severe accident. Part I: Experimental results of the PHEBUS FPT2 test.” *Journal of Nuclear Materials* 453, no. 1-3: 340–354.

[70] Robb, K. R., L. J. Ott, and M. Howell. (2018) “Design and analysis of oxidation tests to inform FeCrAl ATF severe accident models.” Tech. Rep. ORNL/SPR-2018/893. Oak Ridge National Laboratory.

[71] Sakamoto, K., et al., (2021) “Development of accident tolerant FeCrAlODS fuel cladding for BWRs in Japan.” *Journal of Nuclear Materials* 557: 153276.